LEGIBILITY NOTICE

A major purpose of the Technical Information Center is to provide the broadest dissemination possible of information contained in DOE's Research and Development Reports to business, industry, the academic community, and federal, state and local governments.

Although a small portion of this report is not reproducible, it is being made available to expedite the availability of information on the research discussed herein.

CONF-8405529--11

LA-UR-84-1279
CONF

NOTICE

PORTIONS OF THIS REPORT ARE ILLEGIBLE. It has been reproduced from the best available copy to permit the broadest possible availability.

Los Alamos National Laboratory is operated by the University of California for the United States Department of Energy under contract W-7405-ENG-36

LA-UR--84-1279

DE84 011327

TITLE: A GENERAL-PURPOSE RFQ DESIGN PROGRAM

AUTHOR(S): E. A. Wadlinger, AT-2

SUBMITTED TO: The 1984 Linear Accelerator Conference, May 7-11, 1984
Darmstadt, Fed. Rep. of Germany

DISCLAIMER

MASTER

Los Alamos Los Alamos National Laboratory
Los Alamos, New Mexico 87545

GENERAL-PURPOSE RFQ DESIGN PROGRAM*

E. A. Wadlinger, AT-2, MS-H811
Los Alamos National Laboratory, Los Alamos, New Mexico 87545

Summary

We have written a general-purpose, radio-frequency quadrupole (RFQ) design program that allows maximum flexibility in picking design algorithms. This program optimizes the RFQ on any combination of design parameters while simultaneously satisfying mutually compatible, physically required constraint equations. It can be very useful for deriving various scaling laws for RFQs. This program has a "friendly" user interface in addition to checking the consistency of the user-defined requirements and is written to minimize the effort needed to incorporate additional constraint equations. We describe the program and present some examples.

Introduction

There are many different criteria that can be used to optimize a particular RFQ. We might maximize the brightness for a given current, or maximize the current for a given brightness while minimizing particle loss and vane-tip activation. We might constrain the overall length and power requirements for the design, or maintain a given betatron and synchrotron tune through the structure.

We do not wish to write a separate program to handle every new approach to RFQ design. Therefore, we have written a program that automates the design for RFQ accelerators, optimizes arbitrary given parameters while fixing others, and satisfies the constraint equations governing the physics. The program does a least-squares optimization of parameters coupled with a Lagrange multiplier method to handle the constraint equations.

In the next section, we define the problem for designing RFQs and present a solution. We then give an overview and several examples of the program "RFQDES." A friendly user interface and a table that checks the consistency of the users requirements is still being developed. When fully developed, the program will pick the appropriate set of constraint equations, given a set of requirements.

Method

RFQDES was written both to automate the design process for RFQ accelerators and to increase the flexibility of our traditional design process.[1] We design the accelerator by optimizing the design on certain parameters (desired current, emittance, emittance/acceptance ratio, energy gain per cell, longitudinal and transverse space-charge parameters) while simultaneously subjecting these parameters as well as other parameters (vane modulation, minimum vane radius, synchronous phase, betatron and synchrotron tunes, etc.) to design and physics constraints.

We solve this problem by defining a function I that is the squared sum of the (fitted minus desired) parameter values plus the sum of the constraint equations multiplied by Lagrange multipliers. The function I is then minimized by taking derivatives of the function with respect to all the nonfixed parameters of the system. The resulting equations, which are highly nonlinear, are solved with the Newton-Raphson technique.

All parameters can be placed in one of three categories: (1) fixed, (2) optimized about a desired value, or (3) free floating. Fixed parameters are ignored in the following derivation. They are treated as fixed numerical constants in the constraint equations. Optimized parameters are denoted by X_a where a is an index for the X variable array. Free-floating parameters are denoted by Y_i and i is the corresponding index of this array. We define the following parameters and functions:

X^d = the desired values for parameters X

X^f = the fitted values for the parameters X

σ_a = the weight parameter for X_a

Y = the RFQ floating variables (no desired or fixed value)

α_λ = the Lagrange multiplier for the λ^{th} constraint equation

F_λ = the λ^{th} constraint equation

$F_{\lambda,a} = \partial F_\lambda / \partial X_a$

$F_{\lambda,i} = \partial F_\lambda / \partial Y_i$

We define an effective chi-square function I where

$$I = 1/2\left[\sum_a \frac{\left(X_a^f - X_a^d\right)^2}{\sigma_a^2} + 2\sum_\lambda \alpha_\lambda F_\lambda(x^f, y)\right] \quad . \tag{1}$$

We minimize I with respect to X, Y, and α, and obtain the following set of nonlinear equations:

$$J_a = \partial I/\partial X_a = (X_a^f - X_a^d)/\sigma_a^2 + \sum_\lambda \alpha_\lambda F_{\lambda,a} = 0 \quad , \tag{2}$$

$$J_i = \partial I/\partial Y_i = \sum_\lambda \alpha_\lambda F_{\lambda,i} = 0 \quad , \text{ and} \tag{3}$$

$$J_\lambda = \partial I/\partial \alpha_\lambda = F_\lambda = 0 \tag{4}$$

for all a, i, and λ indices. (If there are A optimized parameters, I free-floating parameters and Λ constraint equations, then $(1 \le a \le A)$, $(1 + A \le i \le A + I)$, and $(1 + A + I \le \lambda \le A + I + \Lambda)$. We solve the system of eqs. (2 to 4). We obtain the matrix equation

$$J^{n+1} = J^n + [\partial J/\partial(X,Y,\alpha)|_n]$$

$$* [(X^{n+1}, Y^{n+1}, \alpha^{n+1}) - (X^n, Y^n, \alpha^n)] = 0 \quad , \tag{5}$$

which can be inverted to give

$$(X^{n+1}, Y^{n+1}, \alpha^{n+1}) = (X^n, Y^n, \alpha^n) - [\partial J/\partial(X,Y,\alpha)|_n]^{-1}$$

$$* (J^n) \tag{6}$$

where n and n + 1 denote the iteration number.

*Work supported by the US Department of Defense, Defense Advanced Research Projects Agency, and Ballistic Missile Defense Advanced Technology Center.

Program RFQDES Overview

We adhered to the FORTRAN 77 standard in writing RFQDES. The structure is modularized to facilitate implementing future changes. All derivatives are calculated analytically to improve the precision and rate of convergence of the Newton-Raphson technique. We used the chain rule for taking derivatives so that modifications to a formula for calculating a constraint equation will have a limited or negligible impact on other formulations in the program.

The nonlinear least-squares optimizer routine, though written for this program, was designed so that it can be lifted easily from this package and used elsewhere. Each variable, except in the optimizing package where array variables are used, is given a name that indicates its function. One subroutine is used to convert back and forth between named variables and the array variables needed by the optimizer. This procedure introduces a slight run-time inefficiency but greatly facilitates coding and debugging. The resulting program is more readable and modifiable.

All parameters internal to the code are dimensionless [except for beam current which is scaled by $1/(m_0c^2/e)$.] All lengths are scaled by the rf wavelength, potentials by $1/(m_0c^2/e)$, and electric fields by rf wavelength/(m_0c^2/e). The result is that the user's input data define the system of units.

We assumed a uniformly filled, ellipsoidal charge distribution for calculating the space-charge defocusing force. We also approximated the form factor as

$$f(\text{length/width}) = \text{width}/(3\times\text{length}) \quad \text{(Ref. 1 and 2).} \quad (7)$$

Other space-charge models can be substituted in the program in place of this model.

Examples

We illustrate the code by designing (using different criteria) a single cell for an RFQ. A complete design is an extension to the design of a single cell, and this procedure is automated in the program RFQDES. All cases presented are designed for a 1.0-MeV proton beam in a 425-MHz RFQ. We define the maximum electric field on the RFQ vanes in terms of the Kilpatrick criterion[3] (19.9×10^6 V/M at 425 MHz).

The first two runs given in table I show the effect on the beam-current limit obtained in raising the maximum electric field from 2 to 3 times Kilpatrick. The normalized acceptance for both cases was $2 \times 10^{-6}\pi$ m•rad, with the beam contained in a total normalized emittance of $1.0 \times 10^{-6}\pi$ m•rad. The longitudinal and transverse space-charge μ's were fixed at 0.84 in both cases. For Case 1, the current was maximized, while the accelerating gradient was only weakly optimized. The accelerating gradient for Case 2 was fixed to that obtained for Case 1 (30 kV/cell). The current limit obtained for Case 1 was 0.060 A and for Case 2 was 0.208 A.

There are two reasons for the large increase in current for the same emittance and acceptance. First, the synchronous phase went from -21.8 to -41.3°, which effectively doubles the beam length. Secondly, the increased external electric field made the beam smaller for the fixed emittance. Since the ratio of acceptance/emittance was fixed at 2, the RFQ vanes were brought closer together. This reduced vane radius and increased electric field increased the ponderomotive focusing term (B in Ref. 1), which scales as electric-field/minimum-vane-radius.

Cases 3 and 4 were the same as Case 1 except that the maximum electric field was increased from 2 to 3 times the Kilpatrick field; all other physical parameters were held fixed (that is, the same physical RFQ). The Case 3 acceptance/emittance ratio was 2 (same as Cases 1 and 2), whereas the Case 4 acceptance/emittance ratio was 2.55, which gave the same emittance as Cases 1 and 2 ($1.0 \times 10^{-6}\pi$ m•rad). We see that the current limit for Case 3 compared to Case 1 increased to 0.157 A, but the emittance grew to $1.28 \times 10^{-6}\pi$ m•rad. The current in an emittance of $1.0 \times 10^{-6}\pi$ m•rad is 0.120 A (see Case 4). Case 4 should be contrasted with Case 2.

Conclusion

The above example was meant to show a little of the freedom we have to design RFQs using RFQDES. We can conveniently try many different RFQ design approaches and look at various scaling laws. The code is modular, internally well documented, and has a simple data-flow structure (COMMON is not used). We can, with minimum effort, modify the program as needs change.

References

1. K. R. Crandall, R. H. Stokes, and T. P. Wangler, "RF Quadrupole Beam Dynamics Design Studies," Proc. 1979 Linear Accelerator Conf., Montauk, New York, September 10-14, 1979, Brookhaven National Laboratory report BNL-51134, p. 205 (1980).

2. R. L. Gluckstern, "Space-Charge Effects," in Linear Accelerators, P. M. Lapostolle and A. L. Septier, Eds. (North Holland Publishing Co., Amsterdam, 1970).

3. W. D. Kilpatrick, "Criterion for Vacuum Sparking Designed to Include Both rf and dc," Rev. Sci. Instr. Vol. 28, No. 10, p. 824 (1957).

TABLE I

THE 425-MHz RFQ CELL FOR A 1-MeV PROTON BEAM

Kilpatrick Field	Current (A)	Emittance π m•rad	Sync-Phase (°)	Modulation	Sym-Radius (m)	Vane Voltage (V)	Acceptance/ Emittance	Zero-Current Phase Advance (°) Transverse	Zero-Current Phase Advance (°) Longitudinal
2.00E+00	6.00E-02	1.00E-06	-2.18E+01	1.53E+00	4.92E-03	1.24E+05	2.00E+00	1.39E+01	1.57E+01
3.00E+00	2.08E-01	1.00E-06	-4.13E+01	1.66E+00	2.75E-03	1.15E+05	2.00E+00	4.93E+01	2.33E+01
3.00E+00	1.57E-01	1.28E-06	-5.18E+01	1.53E+00	4.92E-03	1.85E+00	2.00E+00	1.72E+01	2.79E+01
3.00E+00	1.20E-01	1.00E-06	-5.18E+01	1.53E+00	4.92E-03	1.85E+00	2.55E+00	1.72E+01	2.79E+01

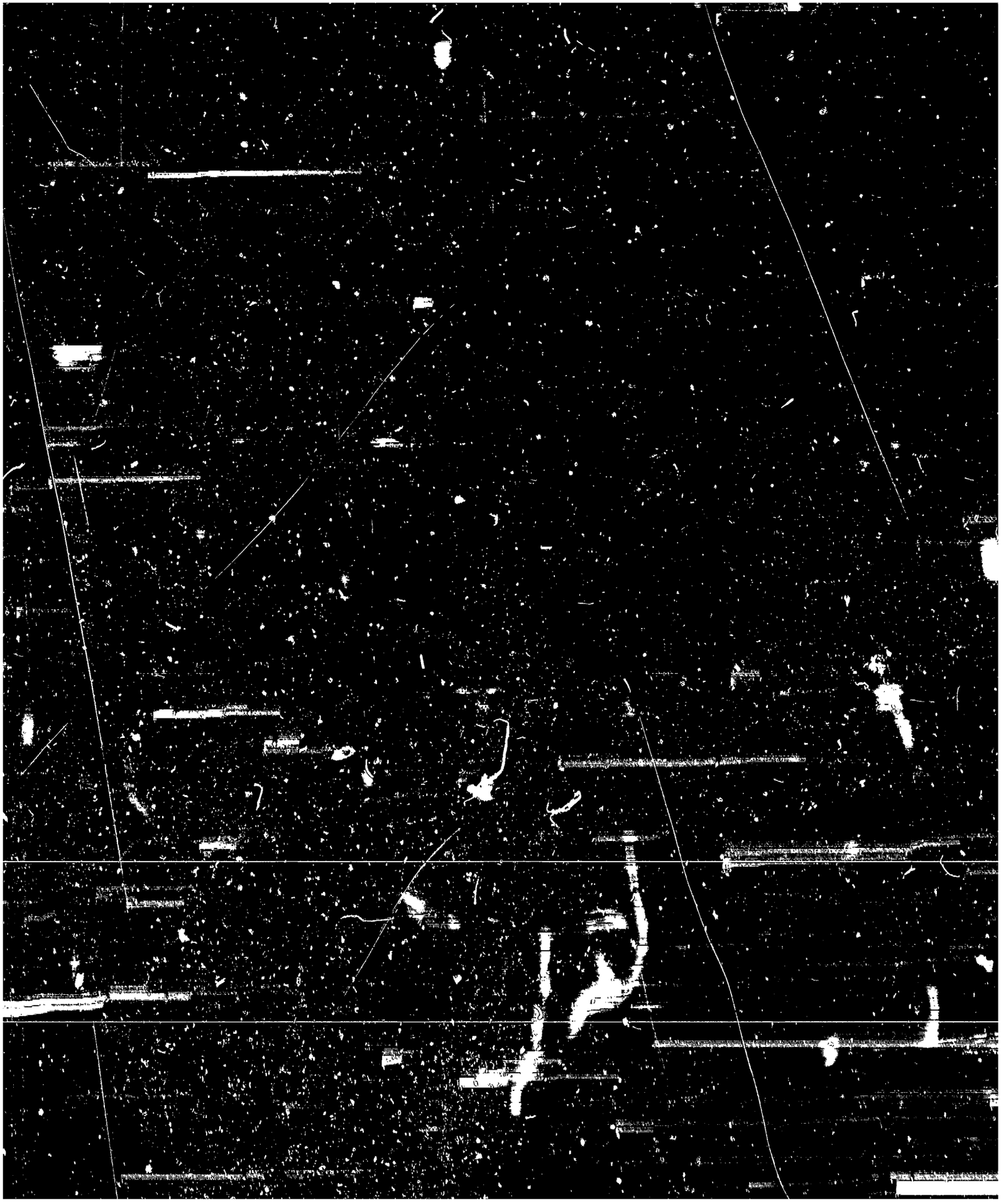

blockage), the resulting value not only falls below that for α' but also out of the range of solutions given by the parabola.

The calculations above are representative of all runs for which this technique has been applied. The accelerational pressure change, predicted based on homogeneous flow, is much higher than that which actually occurs. This is consistent with the effects of slip as discussed in Section III; the presence of slip causes friction to represent a greater portion of the overall pressure change.

In order to apply the technique just described, it is necessary to measure the drag on the cylinder directly, eliminating the correction for acceleration. This has been a standard type of measurement in wind tunnel testing, and a proper technique could be adapted to the present case. Alternatively, a different technique must be developed for measuring the phase dynamic pressures.

APPENDIX A. Supplementary Derivations

Fanno Line Slope

Consider a compressible flow of uniform velocity, in an adiabatic duct of constant cross-sectional area. The energy and continuity equations are

$$d(h + w^2/2) = 0 \quad \text{or} \quad dh = -wdw \tag{A1a,b}$$

$$\frac{dw}{w} = -\frac{d\rho}{\rho}. \tag{A1c}$$

In addition, the Gibbs equation is

$$dh = Tds + vdP \quad \text{or} \quad dP = \rho(dh - Tds). \tag{A2a,b}$$

The process can be considered as a sequence of two processes between the same end states: a throttling process at constant enthalpy, followed by an acceleration process at constant entropy. The pressure differential then can be written as the sum of contributions due to each process:

$$dP = (dP)_s + (dP)_h \tag{A3}$$

where the subscript denotes the property being held constant. Comparison of Eq. (A3) with Eq. (A2b) gives the relation

$$dP_s = \rho dh. \tag{A4a}$$

Substitution for dh from Eqs. (A1b) and (A1c) yields

$$dP_s = w^2 d\rho. \tag{A4b}$$

The density differential can also be written in terms of two contributions. Equation (A4b) is then

$$w^2\left(\frac{d\rho_s}{dP_s} + \frac{d\rho_h}{dP_s}\right) = 1. \tag{A5}$$

The speed of sound a is given by

$$\frac{1}{a^2} = \left.\frac{\partial\rho}{\partial P}\right|_s = \frac{d\rho_s}{dP_s} \tag{A6}$$

and Eq. (A5) becomes

$$1 - M^2 = \frac{d\rho_h}{dP_s} w^2 \tag{A7}$$

where $M = w/a$.

The quantity $d\rho_h$ may be expanded:

$$d\rho_h = \left.\frac{\partial\rho}{\partial P}\right|_h dP_h = \left(-\frac{1}{v^2}\left.\frac{\partial v}{\partial P}\right|_h\right) dP_h .$$

Hence, Eq. (A7) becomes

$$1 - M^2 = -\frac{1}{v^2}\left.\frac{\partial v}{\partial P}\right|_h \frac{dP_h}{dP_s} . \tag{A8}$$

If both sides of this equation are multiplied by $\left.\partial v/\partial P\right|_s$ the result is

$$\frac{1-M^2}{M^2} = \left(\left.\frac{\partial v}{\partial P}\right|_h \Big/ \left.\frac{\partial v}{\partial P}\right|_s\right)\frac{dP_h}{dP_s} . \tag{A9}$$

The quantity $\bar{\gamma}$ will be defined

$$\bar{\gamma} = \left.\frac{\partial v}{\partial P}\right|_h \Big/ \left.\frac{\partial v}{\partial P}\right|_s \tag{A10}$$

and hence the ratio of the pressure change due to dissipation (dP_h) and that due to acceleration (dP_s), from Eq. (A9), becomes

$$\frac{dP_h}{dP_s} = \frac{1-M^2}{\gamma M^2} . \tag{A11}$$

From Eqs. (A2a) and (A3) the following relationship is obtained directly

$$\frac{dP_h}{dP_s} = - \frac{Tds}{dh} \tag{A12}$$

which gives the Fanno line slope:

$$\frac{Tds}{dh} = - \left(\frac{1-M^2}{\bar{\gamma} M^2} \right) . \tag{A13}$$

1. Special case: Ideal gas

Equation (A10) is equivalent to the form

$$\bar{\gamma} = \left. \frac{\partial \rho}{\partial P} \right|_h \Big/ \left. \frac{\partial \rho}{\partial P} \right|_s . \tag{A14}$$

The denominator is just $1/a^2$, where

$$a = \sqrt{\frac{c_p}{c_v} RT} \tag{A15}$$

for an ideal gas. The numerator may be obtained from the ideal gas equation of state,

$$P = \rho RT \tag{A15a}$$

since constant enthalpy implies constant temperatures in this case. Hence:

$$\left. \frac{\partial \rho}{\partial P} \right|_h = \left. \frac{\partial \rho}{\partial P} \right|_T = \frac{1}{RT} . \tag{A15b}$$

and Eq. (A14) becomes

$$\bar{\gamma} = \frac{c_p}{c_v} . \tag{A16}$$

2. Special case: Homogeneous two-phase mixture

The quantity $\bar{\gamma}$ is given by Eq. (A10) in the general form

$$\bar{\gamma} = \left.\frac{\partial v}{\partial P}\right|_h \Big/ \left.\frac{\partial v}{\partial P}\right|_s . \tag{A17}$$

Transformation of the numerator, using Jacobians, to independent variables (P,s) results in

$$\bar{\gamma} = \left\{\left.\frac{\partial v}{\partial P}\right|_s \left.\frac{\partial h}{\partial s}\right|_p - \left.\frac{\partial v}{\partial s}\right|_p \left.\frac{\partial h}{\partial P}\right|_s\right\} \Big/ \left\{\left.\frac{\partial h}{\partial s}\right|_p \left.\frac{\partial v}{\partial P}\right|_s\right\} \tag{A17a}$$

$$\bar{\gamma} = 1 - \left\{\left.\frac{\partial v}{\partial h}\right|_p \left.\frac{\partial h}{\partial P}\right|_s\right\} \Big/ \left\{\left.\frac{\partial v}{\partial P}\right|_s\right\} . \tag{A17b}$$

The additional expressions will be used:

$$\left.\frac{\partial h}{\partial P}\right|_s = v , \tag{A18a}$$

$$\left.\frac{\partial v}{\partial P}\right|_s = -v^2 \frac{1}{a^2} = -\frac{1}{\psi_c^2} \tag{A18b}$$

$$\left.\frac{\partial v}{\partial h}\right|_p = v_{fg}/h_{fg} . \tag{A18c}$$

The quantity $\bar{\gamma}$ is then expressed in the convenient form:

$$\bar{\gamma} = 1 + v\psi_c^2 \frac{v_{fg}}{h_{fg}} = 1 + \frac{v_{fg}}{v} \frac{a^2}{h_{fg}} . \tag{A19}$$

Governing Equations Including Phase Potential Energy

The governing equations for two-phase flow derived in Section II will be modified to include the potential energy of the horizontal flow. This was discussed very briefly in the text as a basis for introducing the Froude number.

Potential energy is important in two-phase flow when the average heights of each phase, measured from a convenient datum, are not equal in a given cross section of pipe. In a homogeneous phase arrangement irrespective of slip, these heights are equal and correspond to the center line of the pipe. They are not equal in a non-homogeneous arrangement with one phase predominantly present in the upper or lower portion of the cross-section. In the most general case, this is represented by a continuous density gradient. The simplest case is a completely stratified flow with a separate vapor layer above the liquid, each phase moving at a different velocity. The equations will be written, in general, by introducing the average phase heights, y_p. In cases when the flow is not stratified the potential energy terms become negligible compared to the kinetic energy and the equations properly describe the flow as given previously.

The difference in potential energy between phases resulting from flow stratification also gives rise to a difference between the average pressures of each phase. The assumption of uniform temperature will be maintained at this point, but will be discussed in more detail once the basic equations have been derived.

The effect of surface tension will also produce a pressure difference between phases. Such an effect occurs on a length scale much smaller

than that experienced with the type of flow being considered, except in the case of extremely small droplets and bubbles, and will not be considered.

Based on the remarks above, the phase conservation equations will be rewritten. The continuity equation remains unchanged and is given by

$$\psi d(x_p) = d(\rho_p w_p \alpha_p) \tag{A20}$$

or

$$\psi x_p = \rho_p w_p \alpha_p. \tag{A21}$$

The energy balance is given, in a form analogous to Eq. (9),

$$\dot{m}(x_p+dx_p)\{(h_p+dh_p+w_{p/2}^2+d(w_{p/2}^2) + g(y_p+dy_p)\} \tag{A22}$$

$$- \dot{m}x_p\{h_p+w_{p/2}^2+gy_p\} - \dot{m}dx_p\{h_i+w_{i/2}^2 + gy_i\}$$

$$= \dot{q}_p L_i dz - \tau_{ip} L_i dz w_i$$

where g is the gravitational acceleration and y_p and y_i are the average height of the phase and the height of the interface, respectively. The introduction of y_i reflects the fact that mass crosses the phase boundary with a potential energy corresponding to the actual height of the interface. The total change in potential energy occurring with the transferred mass is hence apportioned properly to each phase, as with the interface velocity and corresponding kinetic energy.

When Eq. (A22) is expanded and simplified the result is

$$\psi \frac{d}{d\tilde{z}} \{x_p(h_p+w_{p/2}^2+gy_p)\} = \bar{q}_p - \bar{\tau}_{ip}w_i + \psi \frac{dx_p}{d\tilde{z}} \{h_i+w_{i/2}^2+gy_i\}. \quad (A23)$$

The sum of the equation for the phases yields

$$d\{x(h_g+w_{g/2}^2+gy_g) + (1-x)(h_f+w_{f/2}^2+gy_f)\} = 0 \quad (A24)$$

or

$$d(h_0) = 0. \quad (A25)$$

A center of mass height may be defined

$$y_{cm} = xy_g + (1-x)y_f. \quad (A26)$$

The stagnation enthalpy is then

$$h_0 = h + w_{rms/2}^2 + gy_{cm}. \quad (A27)$$

The phase momentum equation is given by

$$\psi \frac{d}{d\tilde{z}} (x_p w_p) = -\alpha_p \frac{dP_p}{d\tilde{z}} + \bar{\tau}_{pw} + \bar{\tau}_{pi} + \psi \frac{dx_p}{d\tilde{z}} w_i \quad (A28)$$

which is derived in exactly the same way as Eq. (39) and is identical except that pressures of the individual phases will be distinguished by a subscript, since in general they will not be equal. Summation of Eq. (A28) for both phases yields

$$\psi \frac{d}{d\tilde{z}} \{xw_g + (1-x)w_f\} = -\alpha \frac{dP_g}{d\tilde{z}} - (1-\alpha) \frac{dP_f}{d\tilde{z}} + \bar{\tau}_{gw} + \bar{\tau}_{fw}. \quad (A29)$$

When the phase pressures are the same, this equation becomes

$$\psi \frac{d}{d\bar{z}} \{w_{cm}\} = -\alpha \frac{dP}{d\bar{z}} + \bar{\tau}_{gw} + \bar{\tau}_{fw} \tag{A30}$$

as obtained previously.

The phase Gibbs equation is just

$$dh_p = T\, ds_p + \frac{dP_p}{\rho_p} . \tag{A31}$$

When this is combined with the phase momentum and energy equations (Eq. (A28) and (A23)) the result is

$$\psi x_p \left\{ T \frac{ds_p}{d\bar{z}} \right\} = \bar{q}_p + \bar{\tau}_{ip}(w_p - w_i) + \bar{\tau}_{wp} w_p \tag{A32a}$$

$$+ \psi \frac{dx_p}{d\bar{z}} (h_i - h_p)$$

$$+ \psi \frac{dx_p}{d\bar{z}} (w_{i/2}^2 - w_{p/2}^2)$$

$$+ \psi \frac{dx_p}{d\bar{z}} g(y_i - y_p)$$

$$+ \psi \frac{dx_p}{d\bar{z}} (w_p - w_i) w_p$$

$$- \psi x_p g \frac{dy_p}{d\bar{z}} .$$

This equation is analogous to Eq. (43), and includes the difference in potential energy between the mass entering and that of the phase. The last

term expresses the change in height of the phase and the resulting contribution of the potential energy change to the phase entropy change. The velocity terms may be combined here also to produce the term

$$(w_p - w_i)^2/2, \tag{A32b}$$

and hence an equation analogous to Eq. (46).

When the phase Gibbs free energy g_p is introduced and Eq. (A32a) is summed for both phases, the result is

$$\psi T \frac{ds}{d\tilde{z}} = \bar{\tau}_{w_g} w_g + \bar{\tau}_i (w_g - w_f) + \bar{\tau}_{w_f} w_f \tag{A33}$$

$$+ \psi \frac{dx}{d\tilde{z}} \{g_f^o - g_g^o\}$$

$$+ \psi \frac{dx}{d\tilde{z}} (w_g - w_i) w_g + \psi \frac{dx}{d\tilde{z}} (w_i - w_f) w_f$$

$$- \psi x g \frac{dy_g}{d\tilde{z}} - \psi (1-x) g \frac{dy_f}{d\tilde{z}}$$

where, in general,

$$g_p^o = g_p + w_p^2/2 + g y_p. \tag{A34}$$

Equation (A33) is analogous to Eq. (48). The additional terms $g dy_p$ represent the changes in potential energy of the individual phases. By combining all velocity terms on the right-hand side of (Eq. A33), the equation may be written as

$$\psi T \frac{ds}{d\tilde{z}} = \bar{\tau}_{w_g} w_g + \bar{\tau}_i (w_g - w_f) + \bar{\tau}_{w_f} w_f \qquad \text{(A35)}$$

$$+ \psi \frac{dx}{d\tilde{z}} \{g'_f - g'_g\} - \psi x g \frac{dy_g}{d\tilde{z}} - \psi(1-x) g \frac{dy_f}{d\tilde{z}}$$

where

$$g'_p = g_p - (w_p - w_i)^2/2 + g y_p. \qquad \text{(A36)}$$

The definitions of g^o_p and g'_p may be modified by introducing the interface property g_i, in addition to w_i and y_i. In this case the former definitions become

$$g^o_p = (g_p - g_i) + (w^2_{p/2} - w^2_{i/2}) + g(y_p - y_i) \qquad \text{(A37a,b)}$$

$$g'_p = (g_p - g_i) - (w_p - w_i)^2/2 + g(y_p - y_i).$$

The additional terms simply cancel in Eqs. (A35) and (A33). The quantity g_i represents the free energy of mass entering a phase at the intermediate interface state. It is also equal to the free energy of either individual phase at the interface, since equilibrium and saturation conditions exist at this point. It will be demonstrated shortly that the phases at other locations may not be at saturation conditions.

In order to understand the role of the kinetic and potential energy terms in relation to the free energy, consider the special case of a two-phase flow which is completely stratified, with vapor alone in the top portion of the cross section, liquid alone in the bottom. The

difference between free energy of either phase and free energy at the interface may be calculated from the equation

$$dg = -sdT + \frac{dP}{\rho} . \tag{A38}$$

The difference in pressure between the interface and the average height of the phase is given by

$$P_p - P_i = \int dP = -\int \rho_p g dy = \rho_p g(y_i - y_p) . \tag{A39}$$

Hence, for a uniform temperature we have

$$g_p - g_i = g(y_i - y_p) . \tag{A40}$$

The gravitational terms in Eqs. (A37a,b) correspond directly to a difference between interface and phase free energies due to a <u>difference in pressure</u>. By analogy the kinetic energy terms may correspond to a free energy difference due to a <u>temperature difference</u>, although it is not clear whether the relative or absolute difference is the proper quantity. For present purposes, the former will be assumed, since this results from the combination of all terms involving $\psi\, dx$. Hence, the following condition may be written:

$$g_p - g_i = (w_p - w_i)^2/2 - g(y_p - y_i) \tag{A41}$$

which corresponds to phase "equilibrium" in the presence of differences in kinetic and potential energy, since it results in the elimination of

entropy production associated with the mass transfer process. It also indicates the existence of a temperature difference between phases in a two-phase system whenever a velocity difference exists, in addition to the pressure difference due to individual phase heights. When the condition of Eq. (A41) is satisfied the dissipation equation becomes

$$\psi T \frac{ds}{d\tilde{z}} = \bar{\tau}_{w_g} w_g + \bar{\tau}_i (w_g - w_i) + \bar{\tau}_{w_f} w_f - \psi x g \frac{dy_g}{d\tilde{z}} - \psi (1-x) g \frac{dy_f}{d\tilde{z}} . \qquad (A42)$$

If the differences in pressure and temperature are neglected, the phase free energies may be set equal:

$$g_g = g_f . \qquad (A43a)$$

If, in addition, the interface velocity is assumed to be the average of the phase velocities

$$w_i = \bar{w} \qquad (A43b)$$

then the dissipation equation becomes

$$\psi T \frac{ds}{d\tilde{z}} = \bar{\tau}_{w_g} w_g + \bar{\tau}_i (w_g - w_f) + \bar{\tau}_{w_f} w_f - g \frac{dy_{cm}}{d\tilde{z}} \qquad (A44)$$

where y_{cm} is the center of mass of the flow defined by Eq. (A26). The above equation is most convenient for use with the one-dimensional, two-fluid equations.

APPENDIX B. Description of the Experimental Facility, Calibration, and Measurement Procedure

The research facility which has been constructed is a highly versatile one, allowing the study and analysis of a wide variety of phenomena involving the flow of a fluid at or near its saturation point as well as in the two-phase region. The design and construction of the facility required approximately two years. The detailed decisions involved in that process have been presented in a previous report [40], which should be considered as part of the present dissertation. The object of this appendix is to provide a summary description of the final configuration of the apparatus and the techniques used for the basic measurements presented in Section IV. Both apparatus and techniques were finalized after a period of trial runs. The versatility of the facility will allow many measurements in the future such as those appropriate for investigations of turbulence or choking in two-phase flow, and vertical flow.

An important feature of the facility, setting it apart from others, is that it is dedicated to two-phase flow of a single substance as opposed to the case of two-substance, two-phase flow (i.e., the flow of air and water). The fluid used is dichlorotetrafluoroethane (designated Refrigerant-114 or simply, R-114); this allows two-phase experiments to be carried out at manageable temperatures and pressures, namely, between 0 and 60°C and up to 10 bar, with the proper similarity relationships to various other cases of practical interest involving different fluids.

Physical Arrangement and Operation

A simplified schematic diagram of the system is given in Fig. B1,

which shows only the main fluid path; auxiliary piping and control systems have been omitted for the sake of clarity. The main circuit consists of the vessels A, B, C and D, and the piping indicated by solid lines. The components are arranged in a closed loop containing only R-114 in either its liquid or vapor state. When the system is not in operation, the bulk of the R-114 is stored in tank (D) as a saturated liquid at room temperature, with vapor occupying the rest of the system.

The system operates in a "blowdown," or intermittent mode rather than as a continuous, steady-state loop. A typical experimental run lasts approximately three minutes, with about three hours required for preparation between runs.

At the beginning of a run, liquid is pumped from the storage tank (D) to the accumulator tank (A) and the booster tank (B), and is heated to the desired initial conditions by means of electric immersion heaters (H). Since the tanks contain saturated liquid and vapor, the pressure is adjusted solely by setting the fluid temperature by means of the heaters. The run is started by opening the isolation valves (IV). Liquid then flows from the accumulator (A) through a venturi flow meter (V) and enters the test section (T). The function of the booster tank (B) is to provide superheated vapor to the accumulator (A) through a pressure regulating valve (PR). This will condense very slowly and maintain a predetermined accumulator pressure and thus compressed liquid in the accumulator. Measurements are carried out in the test section (T) as the flow develops from single-phase to two-phase because of throttling and pressure losses. The mixture is converted back to the liquid phase in the condenser (C) and finally collects in the storage (or "dump") tank (D). The condenser is cooled by a methanol-water solution (shown in the

diagram by dashed lines) from a cold storage tank (CS) which is maintained at a predetermined temperature (approximately -20°C) by a standard refrigeration chiller (CH). The chiller uses city water as its heat sink.

The compressed liquid working fluid, close to saturation, enters the 2 inch diameter test section from a larger diameter settling chamber. Two-phase flow is produced in the test section by the natural decrease in pressure due to friction, or by an orifice plate if more throttling is required. Temperature and differential pressure measurements are taken at successive stations along the test section. The entire 2 inch diameter portion is transparent Pyrex glass, thus allowing direct observation of the flow. The flow rate and conditions in the test section are controlled by the size of the orifice and the setting of the gate valve. Finally, the fluid passes through a diffuser and into a return pipe which leads to the condenser.

The facility occupies portions of the basement and first floor of the laboratory. Plan views and a section are given in Fig. B2(a) and B2(b).

Test Section

A schematic of the test section is shown in Fig. B3. The test section proper is located between two isolation valves. With the exception of mass flow rate, all experimental measurements and observations are made between these two valves. They are of the butterfly type and are pneumatically controlled for fast operation either by hand or automatically by the computer. The valves are always either fully open or closed and are not used to condition the flow in the test section in any

way. The upstream valve isolates the settling chamber from the pipe leading from the venturi flow meter, whereas the downstream valve isolates the diffuser from the return pipe and the condenser.

The settling chamber has a 5 inch diameter. An insert of machined plastic (Delrin), provides a smooth transition to the 2 inch diameter glass portion of the test section, consisting of a series of tubes of various lengths connected to one another by means of clamps fitted at flanged ends. The lengths range from 1 ft to 4 ft, with 4 ft between the primary measuring stations.

At the end of the test section a gate valve and diffuser are connected to the condenser by means of the return pipe. The diffuser provides an expansion in diameter from 2 inches to 5 inches.

The settling chamber and the fixed support mentioned above are mounted on a 6 inch square aluminum I-beam which runs the full length of the test section. The glass sections are supported on this beam by adjustable stands which clamp onto the beam and allow alignment of the glass. The test section is supported separately and connected properly to other piping to eliminate vibration. The total length of the transparent section is 24 ft.

Pressure and temperature transducers are accommodated along the test section in special fittings: Delrin inserts fit between the ends of the glass sections and have an inside diameter matching that of the glass pipe.

Pressure transducers are connected by plastic tubing to a brass fitting which screws into a well in the insert, with a small hole connecting the well to the inside wall of the insert. Hence, static pressure is measured at the wall. Both absolute and differential transducers

are connected using this arrangement.

Temperature probes are mounted in a brass fitting which screws into the insert and allows the probe to be positioned radially.

A temperature and absolute pressure transducer are connected similarly at the settling chamber, with fittings screwed into the steel pipe wall.

Flow control for the test section is accomplished by four devices: a throttle plate, a throttle valve, and two isolation valves. The latter are used only as shut-off valves, as mentioned above.

The throttle plate is an aluminum disc with a number of holes drilled to provide a specified total flow area. The disc is clamped in an aluminum holder which fits between two glass sections, in the same manner as the Delrin inserts. Control of the flow is accomplished by causing the liquid to choke at the plate. In this way, the flow rate can be held nearly constant during the run, regardless of changes which occur in the flow further downstream. The downstream gate valve is adjusted to control the amount of flashing and the type of flow which occurs in the test section, without changing the mass flow rate. Also, the pressure in the diffuser is maintained sufficiently low (by the operation of the condenser) so that the two-phase flow in the test section is choked at the gate valve. Thus, conditions in the test section can be held constant during a run, despite changes which occur in other parts of the system, since the flow occurs between two choked cross sections.

With a throttle plate of a given flow area the mass flow rate can be adjusted over a limited range by adjusting the pressure in the accumulator tank. If a larger variation is required, a plate with a different flow area is used. The applied boost is the pressure applied to the

accumulator above the saturation pressure in that tank. The principle of choked liquid flow has been examined in detail and is the subject of a forthcoming report [41].

Some specific characteristics of the test section are illustrated in Fig. B3 and should be noted.

The throttling plate has a total flow area which is determined as outlined above. This flow area is composed of 41 small holes arranged symmetrically in the plate, with a total area corresponding to a single opening of diameter 0.5 inch. It was determined that this number of holes, in conjunction with the 6 ft length before the first measuring station, produced a jet which was dispersed sufficiently to not affect flow in the measuring portion of the test section. A fully developed flow is thus produced before the first measuring point.

The orifice essentially simulates the friction effect which a much longer section of constant area pipe would have, and allows conditions to be produced in the measuring section which would exist at various locations along a pipe of much greater length. The various "locations" are produced by changing the setting of the gate valve to produce more or less flashing immediately following the orifice plate.

Temperature measurements are taken directly by the temperature probes placed as shown in Fig. B3. Differential pressure measurements are taken across each of the 4 ft sections by actually placing differential pressure transducers between the test section and a reference pressure line filled with hydraulic oil, and then calculating the difference between these measurements. This technique is used since connecting the differential transducers directly between stations created long sections of tubing, filled with freon which could change phase during a run,

creating arbitrary, indeterminable pressure fluctuations due to gravity. The reference system allows use of an incompressible liquid in the long sections of tubing, with very short sections connected to the test section. The pressure in the reference line adjusts automatically to a proper value (assuring that all ΔP transducers will be within range) since it is exposed to a pressure at the first measuring station by means of an interface system. The interface consists of a small "U" tube with mercury in its base and oil and freon vapor on opposite sides. The U tube (or "surge pot") is heated to prevent freon inside from changing phase as the pressure fluctuates in the test section. The mass of mercury in the U tube, along with a small air bubble placed at each transducer on the reference side produces a damping effect sufficient to render the reference pressure essentially constant during a run.

Monitoring and Control Instrumentation

During the time the facility is idle, conditions throughout the system are continuously monitored by the computer-controller, a Hewlett-Packard HP-85 desk-top model. This machine is programmed to take action to maintain certain conditions, e.g., operation of the chiller to maintain the cold storage tank at the desired temperature.

During the time the system is being prepared for a test run, the preparation procedure is monitored and controlled by the same computer so that once the desired starting time for the run has been entered into the computer by the operator, all of the required steps will be initiated and controlled automatically (operation of valves, heaters, etc.) assuring that the system will be ready for a run at the prescribed time.

The link between the controller (HP-85) and the physical system is

provided by the HP-IB "Interface Bus" with the Hewlett-Packard Multi-Programmer. These devices allow the computer to read a number of instruments and take action, i.e., operate equipment, by switching relays.

There are two types of measurements taken for automatic control and monitoring purposes: tank temperatures and liquid levels. Temperatures are measured using thermistors attached to the exterior wall of the tank, beneath the insulation. These are located on each of the tanks in the system, including the methanol cold storage tank. Liquid levels are determined by reading differential pressure transducers connected across the top and bottom of the tank to sense hydrostatic pressure, and hence liquid level.

In addition to the above, visual monitoring of temperatures, pressures, and liquid levels is possible, when needed, using standard mercury-in-glass thermometers, dial pressure gauges, and sight glasses.

Data Acquisition Instrumentation

The instrumentation for the experimental measurements consists of three types of sensors: temperature, absolute pressure, and differential pressure. The sensors are of the same basic types as used for the monitoring measurements, but are calibrated and mounted so as to produce the highest accuracy possible.

Although not located in the test section proper, the venturi meter allows measurement of flow rate by means of a differential pressure transducer connected between its inlet and throat sections. Details on the test section instrumentation and the venturi are given later in this appendix.

When preparation for a test run has been completed, measurements are taken in the test section using the controller (HP-85). The computer scans all instruments in the test section, and the venturi, at predetermined time intervals (approximately 1 sec). It is also programmed to control the test run by operating the isolation valves, gate valve, pressure regulating valve and condenser.

Data collected during a test run are stored in the memory of the HP-85 in real time. At the end of the run, the data are transcribed on tape and can be printed in raw form directly, i.e., voltage measurements from each instrument as read in each scan, or in reduced form in units of temperature, pressure, and mass flow rate.

Lastly, a set of programs has been developed to provide additional data reduction and graphic display for calculations made from the measurements, such as values for density ratios, Mach numbers, etc.

Since the facility was designed as an intermittent one with running times of one-half to three minutes, it is clear that for all operations of the facility including the acquisition of data and the running of the experiment, automation was highly desirable, if not an absolute necessity. After investigating a number of options, the Hewlett-Packard HP-85 computer was chosen as the basic controller for the system. This not only satisfied requirements for control and data acquisition, but also made available a reasonably powerful computer for data evaluation and theoretical studies.

Measurement for Experimental Data

1. Temperature Measurement

The sensors selected for measuring temperature were thermistors, a semiconductor material having a resistance which is sensitive to

temperature. The dependence of the resistance on temperature is given by

$$\phi(T) = \alpha e^{-\beta/T}, \tag{B1}$$

where T is the absolute temperature and the constants α and β depend on the material. A known current pulse is passed through the thermistor and ϕ is a voltage measured as a function of temperature.

The specific thermistors were selected based on their sensitivity over the required temperature range and an output which is compatible with the A to D voltage conversion equipment. The manufacturer's specifications were used for the selection process. A method for mounting was designed and implemented, and calibrations were then carried out for each thermistor.

Because of the way the thermistor had to be mounted (i.e., in a fluid flow, and along the radius of a circular cross section), the type selected was a glass-coated bead with adjacent leads. This allowed the thermistor to be mounted as shown in Fig. B4, with the leads passing through a sealed tube. The tube is held in a fitting attached to a Delrin pipe insert and allows the tube to be positioned radially and locked in place.

Thermistors with resistance values at 25°C of either 1 kΩ or 2 kΩ are presently in use. With an applied measuring current of 200 μA, the resulting voltage is between 0 and 1 V over the calibration temperature range of 0 to 30°C. The 1 kΩ thermistors allow temperatures lower than 0°C to be measured when needed, without exceeding 1 V output of the A-D converter.

Calibration of the temperature transducers was carried out using a heated, thermostatically-controlled water bath. Points were taken at approximately 3°C intervals over the calibration range. A computer program has been written which allows the HP-85 to read the transducer output voltage at each point. The corresponding temperatures, read on a precision mercury-in-glass thermometer with increments of 0.1°C, are provided by the operator. The computer then correlates the data for $\phi(T)$ using a least-squares analysis. The form of the correlating equation is obtained from the resistance equation above as

$$\frac{1}{T} = A + B \ln \phi , \qquad (B2)$$

where

$$A = \frac{\ln \alpha}{\beta} \quad \text{and} \quad B = -\frac{1}{\beta} . \qquad (B3)$$

A sample correlation is given in Fig. B5, showing the input data, resulting correlation equation, standard deviation, and deviation of data from the smooth curve.

2. Absolute and Differential Pressure Measurement

The type of probe selected for measuring absolute and differential pressure is an integrated circuit pressure transducer† which provides a voltage output that is linear with the applied pressure or pressure difference. The transducer consists of a single-crystal silicon sensor and circuit elements mounted in a ceramic housing. Attached directly to the

†Supplier: SenSyn Company, Sunnyvale, California. Formerly National Semiconductor.

housing are ports of brass tubing for connection to the pressure source, and electrical connections for a 15-volt excitation signal and output voltage. For this application, it was decided to mount the transducer in a metal box, as shown in Fig. B6, which allows the transducer to be isolated from stress created by the external tubing and electrical connections.

The differential pressure transducers selected have a range of $\Delta P = -5$ to $+5$ lbf/in^2 (-30 to +30 kPa) with a voltage output in the range 0 to 12 volts, and an offset of approximately 7 V when $\Delta P = 0$.

Calibration is performed over the range -30 to 0 kPa by the use of a program on the HP-85 similar to that used in the temperature probe calibrations. In this case, the low pressure port of the transducer is left open to the atmosphere, and a controlled vacuum is applied to the high pressure port in increments of approximately 7 kPa, as read by the operator on a mercury manometer, accurate to 0.1 mm Hg. Thus, the transducer output is kept in the range $\phi = 0 - 7$ V. The function $P(\phi)$ is correlated by a least-squares analysis to an equation of the form

$$P(\phi) = A + B\phi. \tag{B4}$$

A sample correlation is shown in Fig. B7. The units of pressure are mbar, converted from mm Hg by the computer.

The absolute pressure transducers used have a range of 0-60 lbf/in^2 (0-4 bar). Calibration is accomplished by applying a known pressure to the transducer, as read using a precision bourdon type pressure gauge with increments of 0.1 lbf/in^2. The data is correlated using the same computer program as the differential transducer, and the form of the correlating equation is the same.

3. Mass Flow Rate Measurement

The flow rate is measured by means of a venturi meter which determines mass flow rate by measuring the change in pressure as a flow of liquid passes through a contraction, or throat section. Because of a number of special requirements of this meter, since the fluid is close to saturation, it was decided to design and fabricate the venturi rather than purchase a standard instrument.

The meter consists of an outer tube and flanges made of stainless steel which fit between adjacent pipe flanges in a conventional manner. The throat section is machined from Delrin, and slides into the outer tube. It is held in place by means of two end plates. Sealing, both internally around the throat pressure chamber and externally at the flanges, is accomplished using O-rings. A drawing of the outer tube and insert is given in Fig. B8. There are three interchangeable throat sections, allowing a flow measurement range of about 1 to 21 kg/s, corresponding to a test section mass flux of roughly 400 to 10,000 $kg/m^2 \cdot s$, with throat diameters of 3/4, 1-1/4 and 2 inches.

Measurement of ΔP at the meter is accomplished using a differential pressure transducer of the type discussed earlier, except mounted in a zinc housing (as supplied). It is bolted to a vibration isolator at the venturi and connected by the necessary fittings and valves. The inlet pressure tap is located in the upstream pipe section rather than the venturi unit itself. A temperature probe, of the type discussed earlier, is located at the same position for accurate determination of the fluid density.

Mass flow rate $\dot{m}$ is calculated from the equation

$$\dot{m} = (2\rho\Delta P)^{1/2} A_i \Big/ \left[\frac{A_i^2}{A_t^2} - 1\right]^{1/2}, \qquad \text{(B5)}$$

as derived from Bernoulli's equation. The quantities ρ, ΔP, A_i, A_t are the fluid density, measured pressure difference between inlet and throat, inlet area and throat area, respectively.

The accuracy of the venturi was checked by directly measuring the quantity of fluid which leaves the accumulator tank in a given time period and comparing this to the flow rate measured by the venturi. Calibration data for venturi throat sections 1 and 2, which cover the range of mass flow rate used in the experiments, are given in Figs. B9(a) and B9(b). Mass flow rate measured by the venturi is plotted against the known calculated flow rate. The straight reference lines are lines of equality between these two quantities.

No correction factor on the standard venturi flow equation above has been found necessary, to an accuracy of approximately 2%.

Facility Operation and Measurement Procedure

The process of preparing for an experimental run is always the same, and is controlled by computer program which allows a set of predetermined starting conditions to be attained in the system without manual intervention. Once these have been reached, the system will automatically maintain such conditions until the operator decides to begin the run, when he enters a run "control program." Using the control program, the computer operates the system and takes data based on a set of predetermined, timed actions for controlling the flow and reading the instruments. The waiting period between run preparation and actually starting the test section flow allows very stable conditions to be reached in each part of the system and steady conditions are achieved quickly. The fact that both run preparation and execution are automated allows procedures to be developed and optimized beforehand, and then assures their precise performance. This eliminates operating inconsistencies and possible errors resulting from manual operation. It also allows the operator to monitor measuring systems and observe the flow without being concerned about the instantaneous mechanics of the process.

The run control program has been written in three versions. The type of data required determines the version which is used. A few common features of these programs will be presented before considering their individual details.

The gate valve is first opened to a position selected according to the amount of flashing desired for the run and the accumulator pressure is increased using the booster. Liquid is then allowed to enter the test section slowly, through small diameter tubing which bypasses the inlet isolation valve, until the test section is half full. At this time the

liquid level just covers the thermistor beads and is just below the pressure transducer ports. After a waiting period for equilibrium to be reached, a set of eight scans are taken. A "scan" consists of one measurement from each instrument. With uniform pressure at saturation conditions in the test section, the temperature at the liquid surface will be uniform. Similarly, the difference between test section pressure and reference line pressure will be the same at each measuring station. Pressure difference across the venturi pressure transducer will be zero since no flow exists. These measurements are used for checking consistency between individual temperature and pressure probes, and to provide a reference or "zero" for each probe under known conditions. A correction is applied to all later measurements in a run based on comparison of average readings over four scans. A total of eight are taken to detect any trend which may be present. Absolute pressure and temperature are checked against the known relationship for the fluid at saturation. In addition to calibration, these procedures allow for detection of a problem with any instrument before another run is performed.

Following the referencing procedure, liquid again is allowed to enter the test section slowly until it is full. The methanol pump is then started to reduce the dump tank pressure. At that time flow through the test section is started by opening both isolation valves simultaneously. After a waiting time for the flow to stabilize, a number of measurement scans are carried out, the exact procedure depending on the particular control program. A description of the procedures is given on the pages that follow.

Procedure 1

This program initially sets the gate valve to a position nearly fully open or fully closed. The valve is then opened or closed continuously while a block of scans is taken. In this way a sequence of two-phase flow conditions is produced in the test section in a single run. When measurements are completed, the inlet isolation valve is closed. Once the test section has emptied, the outlet isolation valve is closed and the gate valve reset to closed position.

Procedure 2

The second version of the control program sets the gate valve to a particular position, and this position remains fixed while measurements are taken. A range of flow regimes is examined by setting the valve differently for successive runs. Measurements for versions 1 and 2 showed no difference, indicating that the flow stabilizes quickly under all conditions. For some runs version 2 was modified slightly to include a measurement of void fraction. After the main block of scans were taken, a void fraction probe was inserted, and another set of scans made. Comparison between the two sets give a measurement of void fraction. Details are given in Section III. At the end of the run, the isolation valves are closed simultaneously, and the average void fraction is measured directly by measuring the liquid level, and hence the vapor volume fraction, after applying the proper corrections.

Procedure 3

This version of the control program is a variation of version 1, producing a set of different test section conditions in a single run.

However, the gate valve setting is not changed while measurements are taken. Instead, four blocks of scans are taken. Between each block the isolation valves are closed simultaneously and the gate valve is repositioned. Each time, a waiting period is incorporated between opening the valves (starting the flow) and the start of the measurements.

For runs conducted on the basis of each of the control programs outlined above, subsequent calculations are based on time-averaged data, that is on data averaged over a number of scans. The exception is Procedure 1, where individual scans must be used since conditions vary continuously.

Three series of experimental data were taken. A list of the runs and additional data are provided in the tables. The experimental results are discussed in Section IV.

APPENDIX C. Correlation and Measurement Comparison

The correlation proposed by Lockhart and Martinelli [3] was discussed briefly in the Introduction with relation to other work, past and present, in two-phase flow. It will be compared here to measurements using R-114 from this investigation and with some using R-12 performed by Friedel and Mayinger [31]. The correlation predicts friction pressure change and void fraction. It was obtained based on measurements with two-substance flows using mixtures of air with various liquids, including water and oil. The friction and total pressure change are identical in most such cases since significant acceleration does not occur. The technique was extended to single-substance, evaporating flows in a paper by Martinelli and Nelson [4]. It was assumed that the friction pressure change would be essentially the same as for non-evaporating flow and the total could be obtained by adding the acceleration or "momentum" pressure change required if evaporation occurs. Calculation of this effect requires additional information for slip, or equivalently void fraction. In [4] the phase velocities were calculated both by assuming "no slip" and from the correlation for void fraction Of course the latter is then also assumed to be the same for an evaporating flow. For present purposes experimental data will be compared to the correlated friction pressure change alone, since this is the basis of both papers mentioned above and represents the lower limit for predicted pressure gradient.

The independent variable selected for the correlation and denoted by X is the square root of the ratio of the liquid "superficial"

pressure gradient to that of the vapor. Each is calculated for the phase flowing alone in the pipe at the same mass flow rate as that phase in the two-phase mixture. The corresponding velocity has since been labeled in the literature as the "superficial" phase velocity. It will be denoted here, in general, for phase "p" as

$$w_{sp} = x_p \psi / \rho_p \tag{C1}$$

where ψ is the total mass flux or "mass velocity" of the two-phase flow. The variable X will be denoted by X_M so that it is distinct from the dryness fraction x. The ratio is then

$$X_M^2 = (dP/dz)_{sf} / (dP/dz)_{sg}. \tag{C2}$$

If the friction factor is expressed in the Blasius form (Eq. 78) then in general

$$(dP/dz)_{sp} = \frac{C_B}{Re^n} \rho_p \frac{w_{sp}^2}{2} \frac{1}{D} \tag{C3a}$$

where

$$Re = \rho_p w_{sp} D / \mu_p. \tag{C3b}$$

The constants C_B and n were determined in [3] depending whether

each phase flowed viscously or turbulently in the mixture (n = 1.0 or 0.2, respectively). Hence four different forms of X_M were possible. In [4] only the case with both phases turbulent was considered, with the exponent modified to n = 0.25. For this case, with $\gamma = \rho_f/\rho_g$,

$$X_M^2 = \frac{1}{\gamma} \left(\frac{\mu_f}{\mu_g}\right)^{0.25} \left(\frac{1-x}{x}\right)^{1.75} \tag{C4}$$

which is the form that will be used here.

The independent variable for pressure change is the ratio of the two-phase friction to the superficial liquid pressure gradient,

$$\phi_L^2 = (dP/dz)_{TPF}/(dP/dz)_{sf}. \tag{C5}$$

Values of ϕ_L are given in [3] as a function of X_M, in tabular form. An alternate independent variable ϕ_{LO}^2 introduced in [4] is the same as ϕ_L^2 from Eq. (C5) but with the denominator replaced by the pressure gradient for liquid flow at the total two-phase mass flow rate. Then in terms of ϕ_L,

$$\phi_{LO}^2 \quad \phi_L^2(1-x)^{1.75}. \tag{C6}$$

The term (1-x) may be expressed in terms of X_M and phase properties using Eq. (C4).

If the two-phase friction pressure gradient is replaced by the total, then ϕ_{LO}^2 is essentially the same as ΔP_R introduced for the

presentation of experimental data in Sec. IV. The only difference is that for ΔP_R the liquid pressure gradient in the denominator is calculated using liquid properties μ_f and ρ_f at the flash temperature T^* while for ϕ_{LO} properties at the two-phase temperature are used. For the present experimental data with R-114, ϕ^2_{LO} has been obtained from ΔP_R by correcting for temperature based on the Blasius form of friction factor. The correction becomes

$$\phi^2_{LO} = \Delta P_R \left\{ \left(\frac{\mu^*_f}{\mu_f} \right)^{.25} \frac{\rho_f}{\rho^*_f} \right\} . \qquad (C7)$$

The factor varies only between 1.0 and 0.97 over the experimental temperature range. Hence the correction is less than 3.0%

Experimentally determined values of ϕ^2_{LO} using the total pressure change measurements from Series I, II, III are given in Fig. C1. The Martinelli prediction [3] of friction alone for each series has been shown as a solid line. The measurements for Series II and III exhibit the same change in slope mentioned in Sec. IV.2. The slope increases greatly as the flow pattern changes from stratified to "homogeneous". This transition phenomenon was observed also in data for air-water presented in the discussion at the end of Ref. [3]. In that case, the position of the change in slope varied if the water flow rate were changed. This implies a change of Froud number. Data for Series I and that for Series II and III exhibit a definite symmetry. Each appears to originate from a common line that is nearly horizontal

close to $\phi_{LO}^2 \simeq 2$ but becomes steeper for smaller values of X_M. The position of the change in slope of the line in this case depends on both Froude and Mach numbers. For the air-water data just mentioned, larger Fr moved the change in slope to higher values of ϕ_{LO}, but the data continued to follow closely along the correlation curve. The horizontal shift from Series II and III (Ma $\simeq$ 0.6) to Series I (Ma $\simeq$ 0.3) may be basically a Mach number effect. Plotting this data as a function of X_M is essentially the same as plotting versus v_R, except X_M decreases as v_R (or x) increases. Hence, the influence of Mach number identified in Figs. 10 and 12 will be similar in Fig. C1 for Series II and III, and corresponds to the same type of horizontal shift.

Shown in Fig. C1 is the range of friction pressure change calculated by Friedel and Mayinger [31] based on total pressure change measurements using R-12 in a vertical 1 in. diameter tube. (Details of the calculation were not provided in the paper.) The ϕ_{LO} for friction is larger for this data than for the total pressure change measurements taken using R-114 with stratified flow at the same X_M. This observation agrees, at least qualitatively, with the discussion of Sec. III.1. It was noted there that horizontal stratified flow would be expected to give a much weaker friction force at the interface than would be possible in vertical flow. Calculation of ϕ_{LO}^2 for friction alone from the Martinelli correlation for R-12 has been shown in Fig. C1 as a dashed line, and for R-114 as just mentioned. The correlation in each case exceeds nearly all of the experimental

measurements, including the total pressure change from this investigation. The same has been observed [31] when steam-water data (also single-substance) is compared to the correlation.

The void fraction measurements for Series II and III are shown in Fig. C2. This figure is essentially the same as Fig. 13 except the coordinates are X_M and "holdup" R_L. In terms of void fraction α,

$$R_L = 1 - \alpha. \tag{C8}$$

The correlation for R_L is given in tabular form as a function of X_M in Ref. [3], and is shown in Fig. C2 as a solid line. The reference lines for equal phase dynamic pressures (EDP) and equal phase velocities (no slip, NS) are also shown. The measurements correspond quite closely to the Martinelli prediction, but in general tend to give higher values of R_L (lower α). Within the accuracy of the measurement, all points exceed the correlation. This would be expected for an evaporating versus non-evaporating flow. In the presence of an overall acceleration the denser liquid phase will tend to be accelerated less than the vapor, resulting in greater slip and hence smaller void fraction. This effect seems to be greater for smaller x (larger X_M). The description of the Froude number effect given previously for Fig. 13 also applies to Fig. C2.

A number of other correlations for void fraction have been compared and discussed in detail in a recent report [45].

REFERENCES

[1] Bilicki, Z., DiPippo, R., Michaelides, E.E., Kestin, J. and Maeder, P.F., "Geothermal Two-Phase Flow. A Selective, Annotated Guide to the Literature". Brown Univ. Rep. No. GEOFLO/7, DOE/ET/27225-11, Providence, R.I. (1980).

[2] Gouse, S.W., Jr., "An Index to the Two-Phase Gas-Liquid Flow Literature", M.I.T. Report No. 9, The M.I.T. Press, Cambridge, MA. (1966).

[3] Lockhart, R.W. and Martinelli, R.C., "Proposed Correlation of Data for Isothermal Two-Phase, Two-Component Flow in Pipes", Chem. Eng. Prog. 45, 39(1949).

[4] Martinelli, R.C. and Nelson, D.B., "Prediction of Pressure Drop During Forced-Circulation Boiling of Water", Trans. ASME 70, 695(1948).

[5] Dukler, A.E., Wicks, M. and Cleveland, R.G., "Frictional Pressure Drop in Two-Phase Flow": A. A Comparison of Existing Correlations for Pressure Loss and Holdup", A.I. Ch.E. Journal 10, 38(1964).

[6] Idsinga, W., Todreas, N. and Bowring, R., "An Assessment of Two-Phase Pressure Drop Correlations for Steam-Water Systems", Int. J. Multiphase Flow 3, 401(1977).

[7] Beattie, D.R.H. and Whalley, P.B., "A Simple Two-Phase Frictional Pressure Drop Calculation Method", Int. J. Multiphase Flow 8, 83(1982).

[8] Hughmark, G.A. and Pressburg, B.S., "Holdup and Pressure Drop with Gas-Liquid Flow in a Vertical Pipe", A.I.Ch.E. Journal 7, 677(1961).

[9] Chisholm, D., "A Theoretical Basis for the Lockhart-Martinelli Correlation for Two-Phase Flow", Int. J. Heat Mass Transfer, 10, 1767(1967).

[10] Taitel, Y. and Dukler, A.E., "A Theoretical Approach to the Lockhart-Martinelli Correlation for Stratified Flow", Int. J. Multiphase Flow 2, 591(1976).

[11] Chen, J.J.J. and Spedding, P.L., "An Extension of the Lockhart-Martinelli Theory of Two-Phase Pressure Drop and Holdup", Int. J. Multiphase Flow 7, 659(1981).

[12] Kosterin, S.I., "An Investigation of the Influence of Diameter and Inclination of a Tube on the Hydraulic Resistance and Flow Structure of Gas Liquid Mixtures", Izvest. Akad. Nauk, SSR 12, 1824(1949).

[13] Baker, O., "Simultaneous Flow of Oil and Gas", Oil Gas J. 53, 185(1954).

[14] Hoogendoorn, C.J., "Gas-Liquid Flow in Horizontal Pipes", Chem. Eng. Sci. 9, 205(1959).

[15] Davies, R.M. and Taylor, G.I., "The Mechanics of Large Bubbles Rising through Extended Liquids and through Liquids in Tubes", Proc. Roy. Soc., A200, 375 (1950).

[16] Griffith, P. and Wallis, G.B., "Two-Phase Slug Flow", Trans. ASME, J. Heat Trans. 83, 307 (1961).

[17] Levy, S., "Prediction of Two-Phase Annular Flow with Liquid Entrainment", Int. J. Heat Mass Trans. 9, 171(1966).

[18] Mundhane, J.M., Gregory, G.A. and Aziz, K., "A Flow Pattern Map for Gas-Liquid Flow in Horizontal Pipes", Int. J. Multiphase Flow, 1, 537(1974).

[19] Taitel, Y., Barnea, D. and Dukler, A.E., "Modelling Flow Pattern Transitions for Steady Upward Gas-Liquid Flow in Vertical Tubes", A.I.Ch.E. Journal 26, 345(1980).

[20] Weisman, J., Duncan, D., Gibson, J. and Crawford, T., "Effects of Fluid Properties and Pipe Diameter on Two-Phase Flow Patterns in Horizontal Lines", Int. J. Multiphase Flow 5, 437(1979).

[21] Dukler, A.E., Wicks, M. and Cleveland, R.G., "Frictional Pressure Drop in Two-Phase Flow: B. An Approach Through Similarity Analysis", A.I.Ch.E. Journal 10, 44(1964).

[22] Levy, S., "Prediction of Two-Phase Pressure Drop and Density Distribution from Mixing Length Theory", Trans. ASME J. Heat Trans., 85, 137(1963).

[23] Levy, S., and Healzer, J.M., "Application of Mixing Length Theory to Wavy Turbulent Liquid-Gas Interface", Trans. ASME J. Heat Trans., 103, 492(1981).

[24] Huey, C.T. and Bryant, R.A.A., "Isothermal Homogeneous Two-Phase Flow in Horizontal Pipes", A.I.Ch.E. Journal, 13, 70(1967).

[25] Owens, W.L., Jr., "Two-Phase Pressure Gradient", ASME Int. Devel. Heat Trans., 363(1961).

[26] Maeder, P.F., DiPippo, R., Delor, M. and Dickinson, D., "The Physics of Two-Phase Flow: Choked Flow", Brown Univ. Rep. No. GEOFLO/10, DOE/ET/27225-15, Providence, R.I. (1981).

[27] Bankoff, S.G., "A Variable Density Single-Fluid Model for Two-Phase Flow with Particular Reference to Steam-Water Flow", Trans. ASME J. Heat Trans., 82, 265(1960).

[28] Levy, S., "Steam Slip. Theoretical Prediction from Momentum Model", Trans. ASME J. Heat Trans., 82, 113(1960).

[29] Chesters, A.K., "The Applicability of Dynamic-Similarity Criteria to Isothermal, Liquid-Gas, Two-Phase Flows Without Mass Transfer", Int. J. Multiphase Flow, 2, 191(1975).

[30] Friedel, L. and Mayinger, F., "Scaling of Two-Phase Friction Pressure Drop", Paper B2, European Two-Phase Flow Group Meeting, Harwell, June 1974.

[31] Friedel, L. and Mayinger, F., "Comparison of Two-Phase Friction Pressure Drop in Water and Freon 12, Paper A2, European Two-Phase Flow Group Meeting, Brussels, June 1973.

[32] "Thermohydraulics of Two-Phase Systems for Industrial Design and Nuclear Engineering", Delhaye, J.M. Giot, M. and Riethmuller, M.L., eds., Hemisphere, 1981.

[33] "Advances in Two-Phase Flow and Heat Transfer", Kakac, S. and Ishii, M., eds., Martinus Nijhoff, 1983.

[34] "Two-Phase Flows and Heat Transfer", Kakac, S. and Veziroglu, T.N., eds., Hemisphere, 1977.

[35] Hoogendoorn, C.J. and Buitelaar, A.A., "The Effect of Gas Density and Gradual Vaporization on Gas-Liquid Flow in Horizontal Pipes", Chem. Eng. Sci., 16, 208(1961).

[36] Maeder, P.F., Dickinson, D.A. and Nikitopoulos, D.E., "One Component Two-Phase Flow in Horizontal and Vertical Ducts: Some Basic Considerations", presented at The Ninth Annual Geothermal Reservoir Engineering Workshop, December 13-15, 1983, Stanford University, Stanford, CA.

[37] Lottes, P.A. and Flinn, W.S., "A Method of Analysis of Natural Circulation Boiling Systems", Nuclear Sci. Eng., 1, 461(1956).

[38] "Wind Tunnel Testing", Pope, A., 2nd ed., Wiley, 1954.

[39] "Prandtl, Goettingen Ergebnisse, Part II, Art. 19. As referenced in "Handbook of Engineering Fundamentals", Eshbach, O.W., ed. 13th printing (1949).

[40] Maeder, P.F., Kestin, J., Dickinson, D.A., DiPippo, R. and Olia, H., "Design and Operation of a Two-Phase Flow Research Facility", Brown Univ. Rep. No. GEOFLO/16, LA-UR-82-1838, Prov., R.I. (1982).

[41] Olia, H., Maeder, P.F., DiPippo, R. and Dickinson, D.A., "Two-Phase Fluid Flow Through Nozzles and Abrupt Enlargements", Brown Univ. Rep. No. GEOFLO/19, Prov., R.I. (1983).

[42] Oguchi, K., Reito 52, 869(1977).

[43] "Thermophysical Properties of Refrigerants", ASHRAE Research Project RP-72, Purdue University, 1976. As referenced in ASHRAE Handbook Fundamentals Vol., The American Society of Heating, Refrigerating and Air Conditioning Engineers, New York, N.Y. (1977).

[44] Tkachev, A. G. and Butyrskaya, S. T., "Investigation of the Viscosity of Freons", Fluid Mechanics - Soviet Research 3, 168(1974).

[45] Papathanassiou, G., Maeder, P. F., DiPippo, R. and Dickinson, D. A., "Void Fraction Correlations in Two-Phase Horizontal Flow", Brown Univ. Rep. No. GEOFLO/17, LAUR-83-1902, Prov., R.I. (1983).

[46] Zuber, N. and Findlay, J.A., "Average Volumetric Concentration in Two-Phase Flow Systems", Trans. ASME J. Heat Trans., 27, 453 (1965).

jh
ss
jf

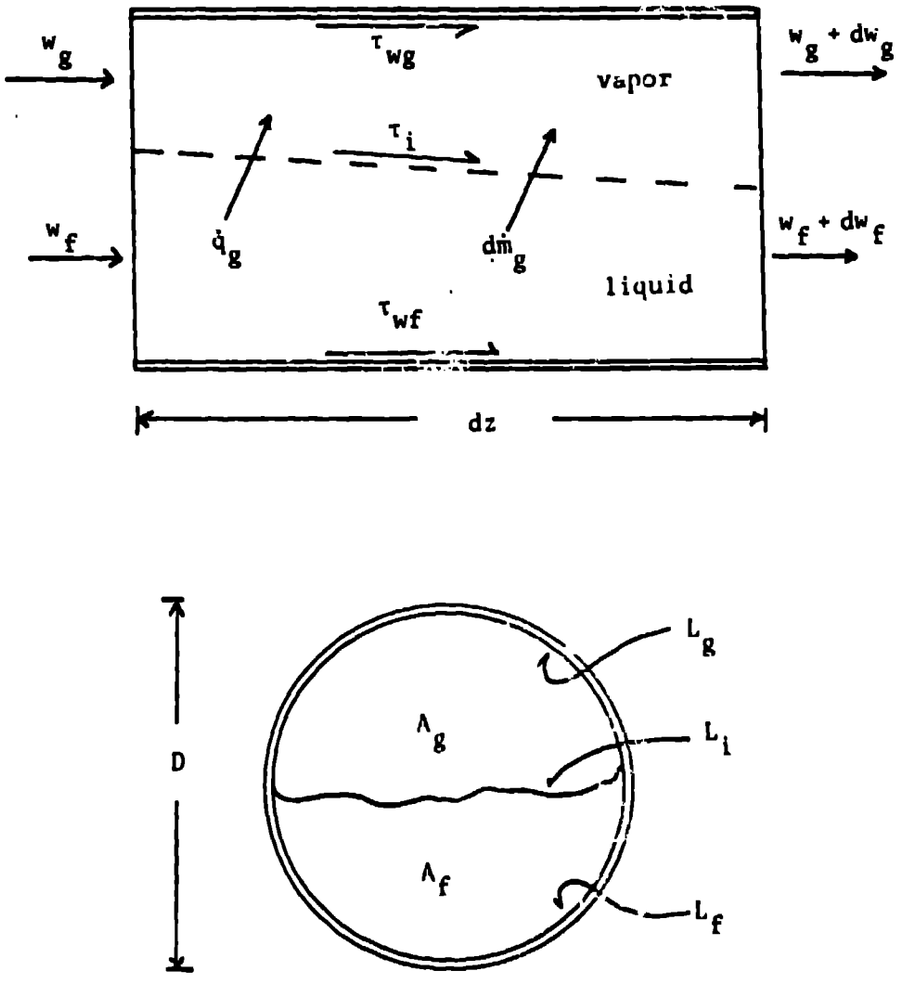
w_g
τ_{wg}
vapor
$w_g + dw_g$
τ_i
w_f
$\dot{q}_g$
$d\dot{m}_g$
$w_f + dw_f$
liquid
τ_{wf}
dz
D
A_g
A_f
L_g
L_i
L_f

FIGURE 1

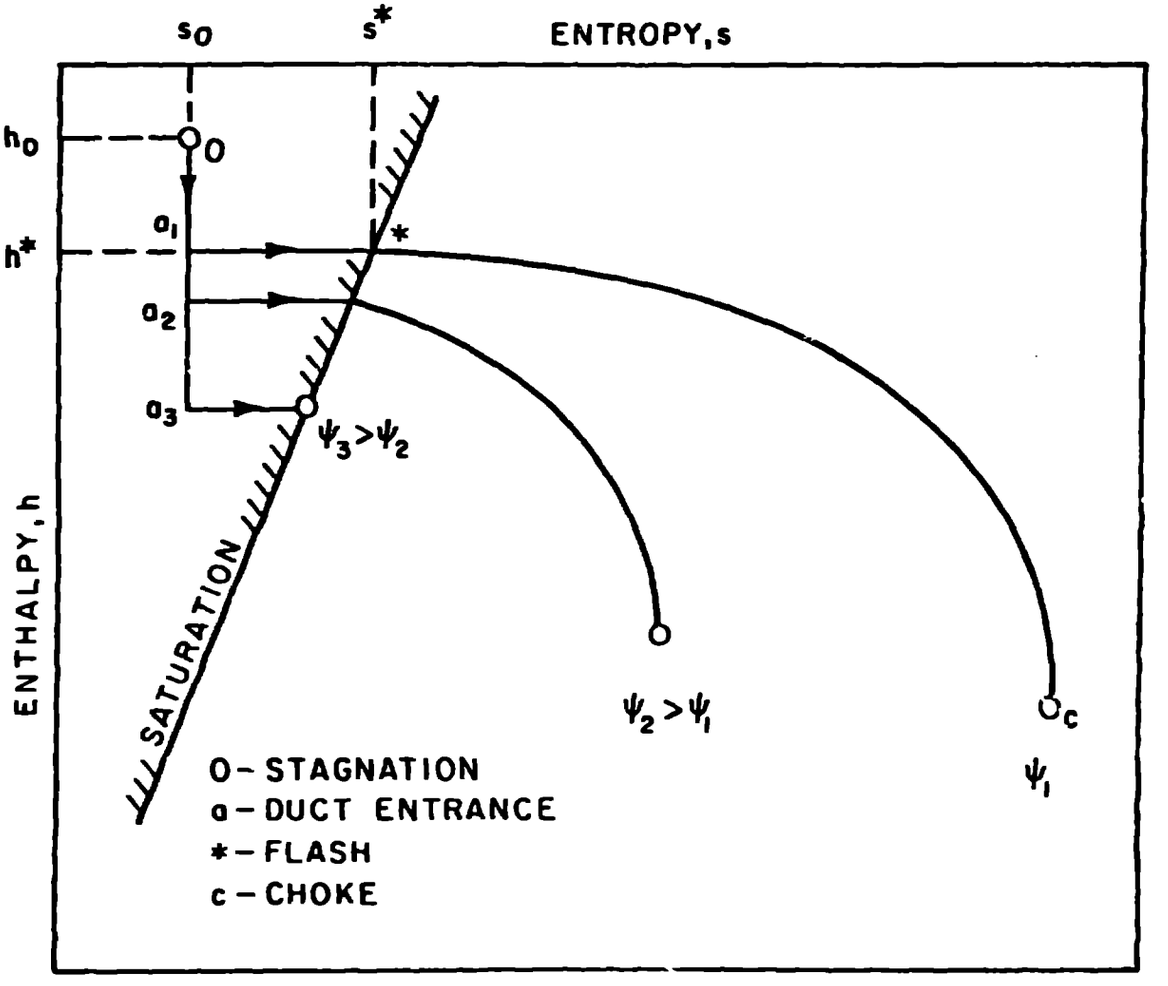
s_0
s^*
ENTROPY, s
h_0
h^*
0
a_1
a_2
a_3
*
$\psi_3 > \psi_2$
$\psi_2 > \psi_1$
c
ψ_1
SATURATION
ENTHALPY, h
0 - STAGNATION
a - DUCT ENTRANCE
* - FLASH
c - CHOKE

FIGURE 2(a)

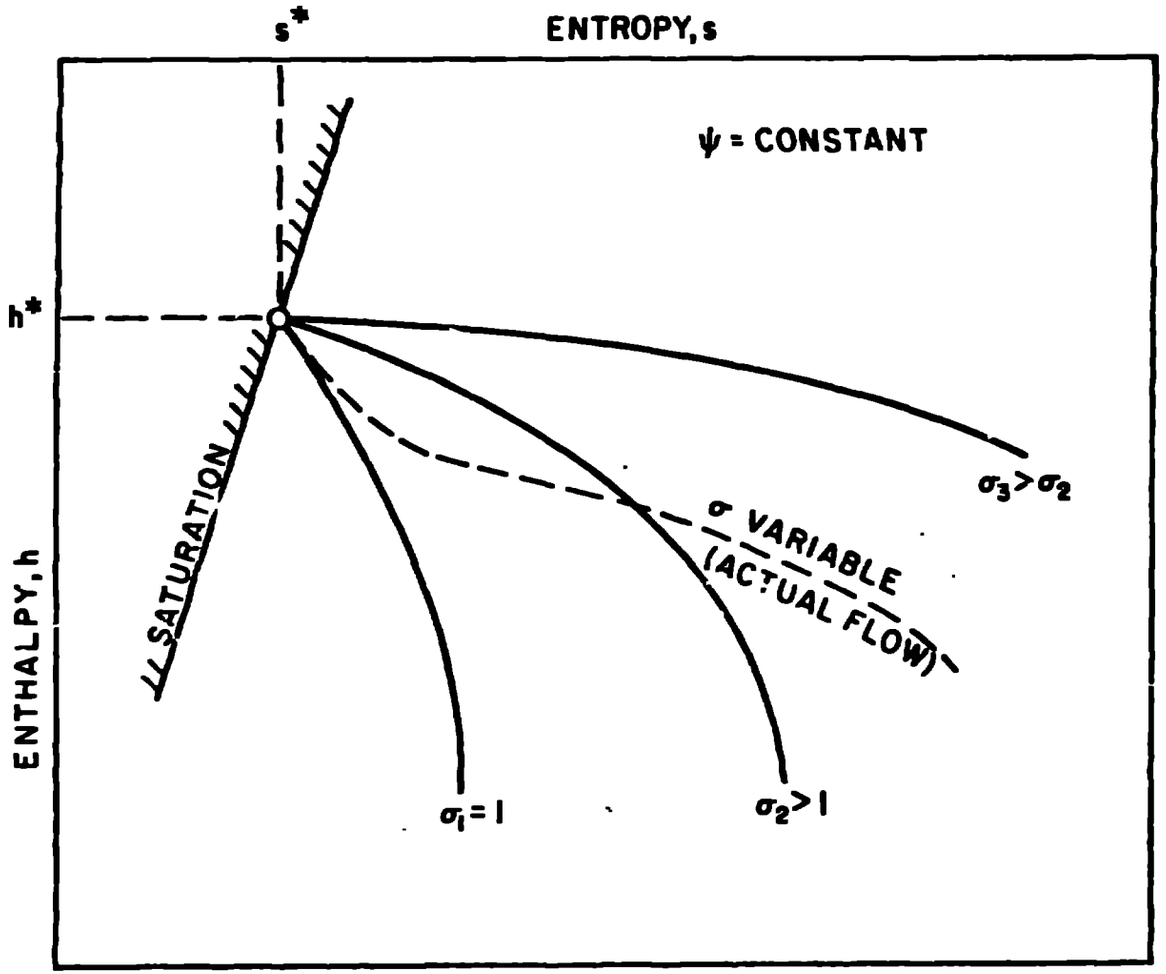
s*
ENTROPY, s
ψ = CONSTANT
h*
SATURATION
σ VARIABLE
(ACTUAL FLOW)
$\sigma_3 > \sigma_2$
$\sigma_2 > 1$
$\sigma_1 = 1$
ENTHALPY, h

FIGURE 2 (b)

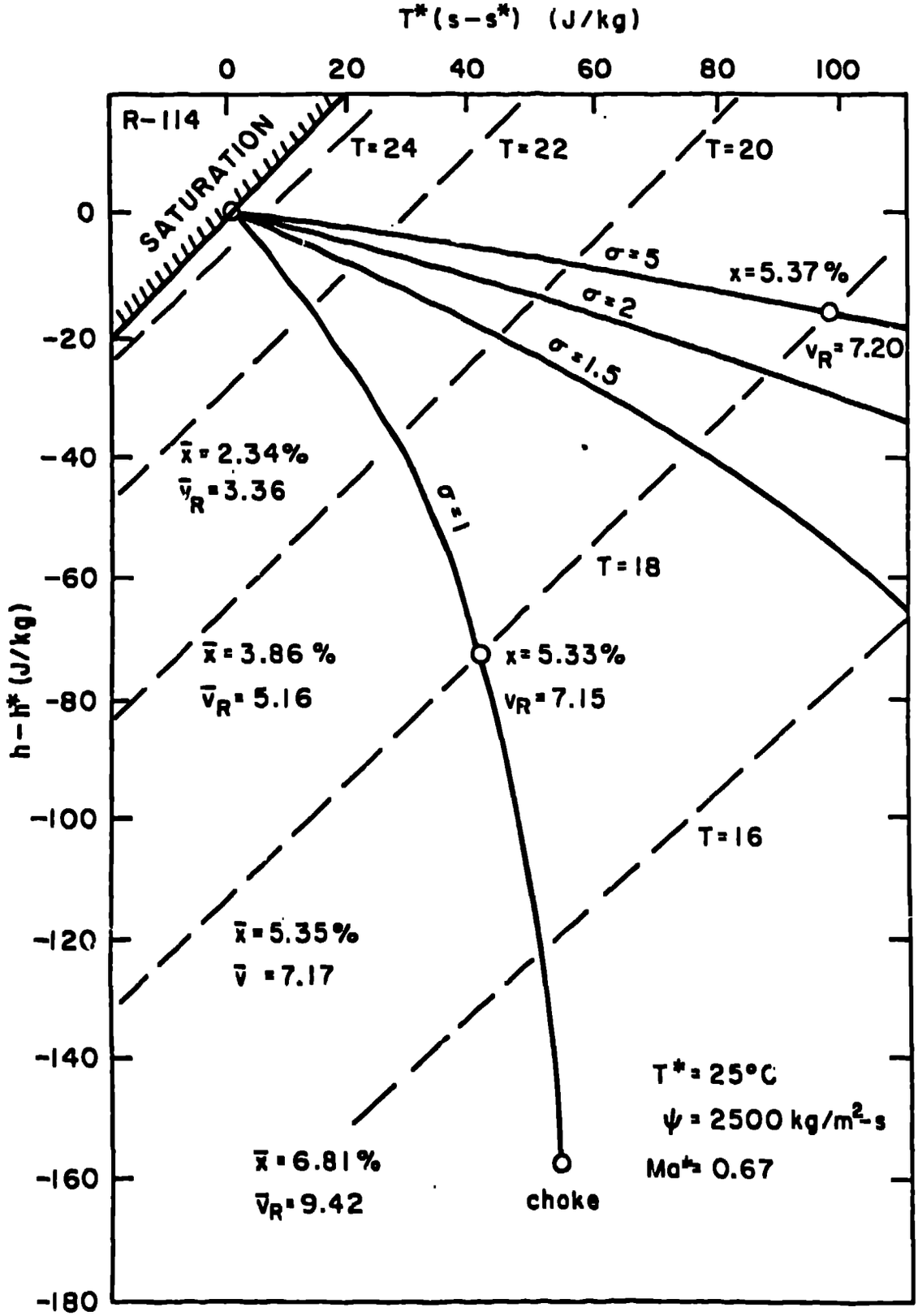
T*(s−s*) (J/kg)
0
20
40
60
80
100
R-114
SATURATION
T=24
T=22
T=20
T=18
T=16
σ=5
σ=2
σ=1.5
σ=1
x=5.37%
v_R=7.20
$\bar{x}$=2.34%
$\bar{v}_R$=3.36
$\bar{x}$=3.86 %
$\bar{v}_R$=5.16
x=5.33%
v_R=7.15
$\bar{x}$=5.35%
$\bar{v}$ =7.17
$\bar{x}$=6.81%
$\bar{v}_R$=9.42
choke
T*=25°C
ψ=2500 kg/m²-s
Ma*=0.67
h−h* (J/kg)
0
-20
-40
-60
-80
-100
-120
-140
-160
-180

FIGURE 3

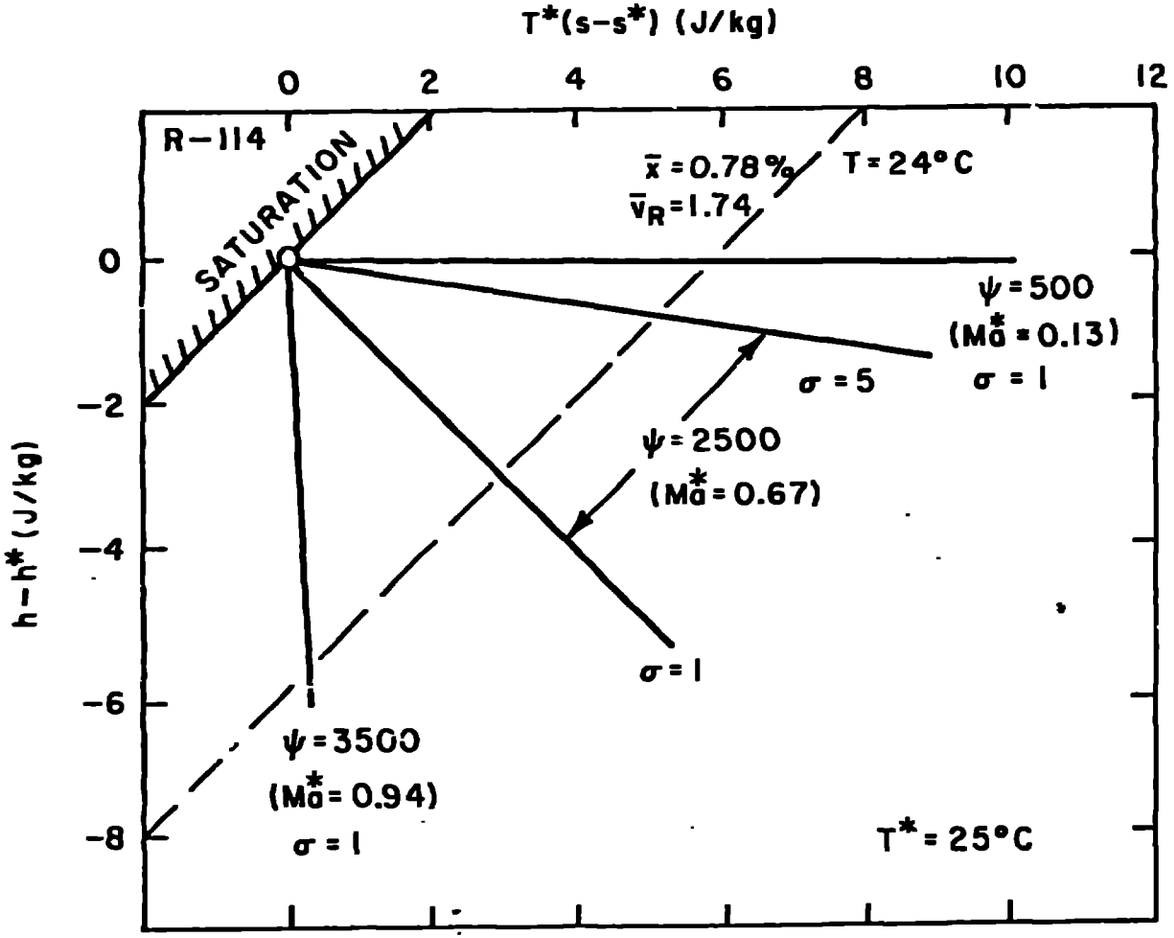
T*(s-s*) (J/kg)
0
2
4
6
8
10
12
R-114
SATURATION
$\bar{x}$ = 0.78%
$\bar{v}_R$ = 1.74
T = 24°C
0
-2
-4
-6
-8
h-h* (J/kg)
ψ = 500
(Mā* = 0.13)
σ = 1
σ = 5
ψ = 2500
(Mā* = 0.67)
σ = 1
ψ = 3500
(Mā* = 0.94)
σ = 1
T* = 25°C

FIGURE 4

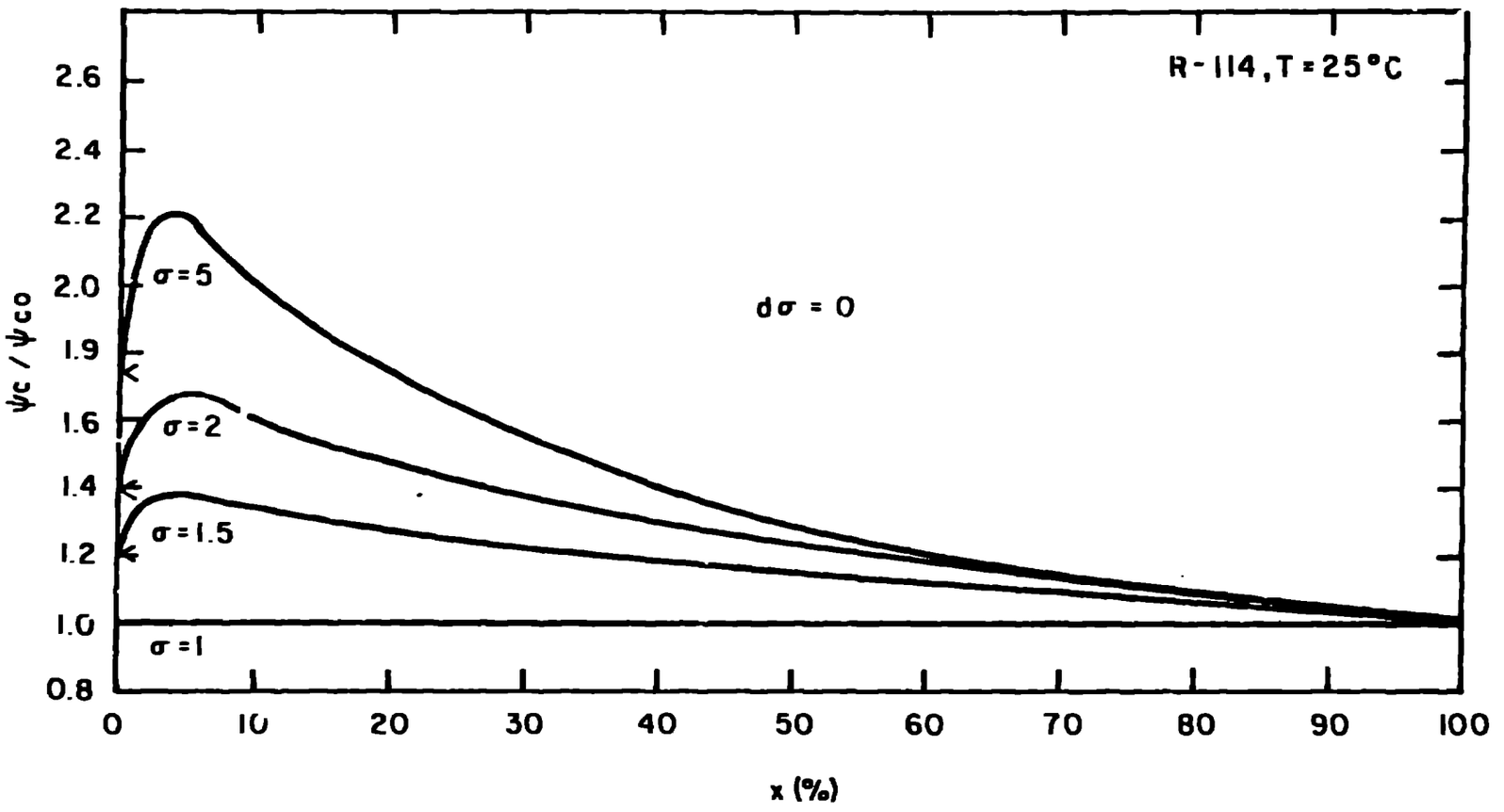
R-114, T = 25°C
dσ = 0
σ=5
σ=2
σ=1.5
σ=1
ψc / ψco
x (%)
2.6
2.4
2.2
2.0
1.9
1.6
1.4
1.2
1.0
0.8
0
10
20
30
40
50
60
70
80
90
100

FIGURE 5

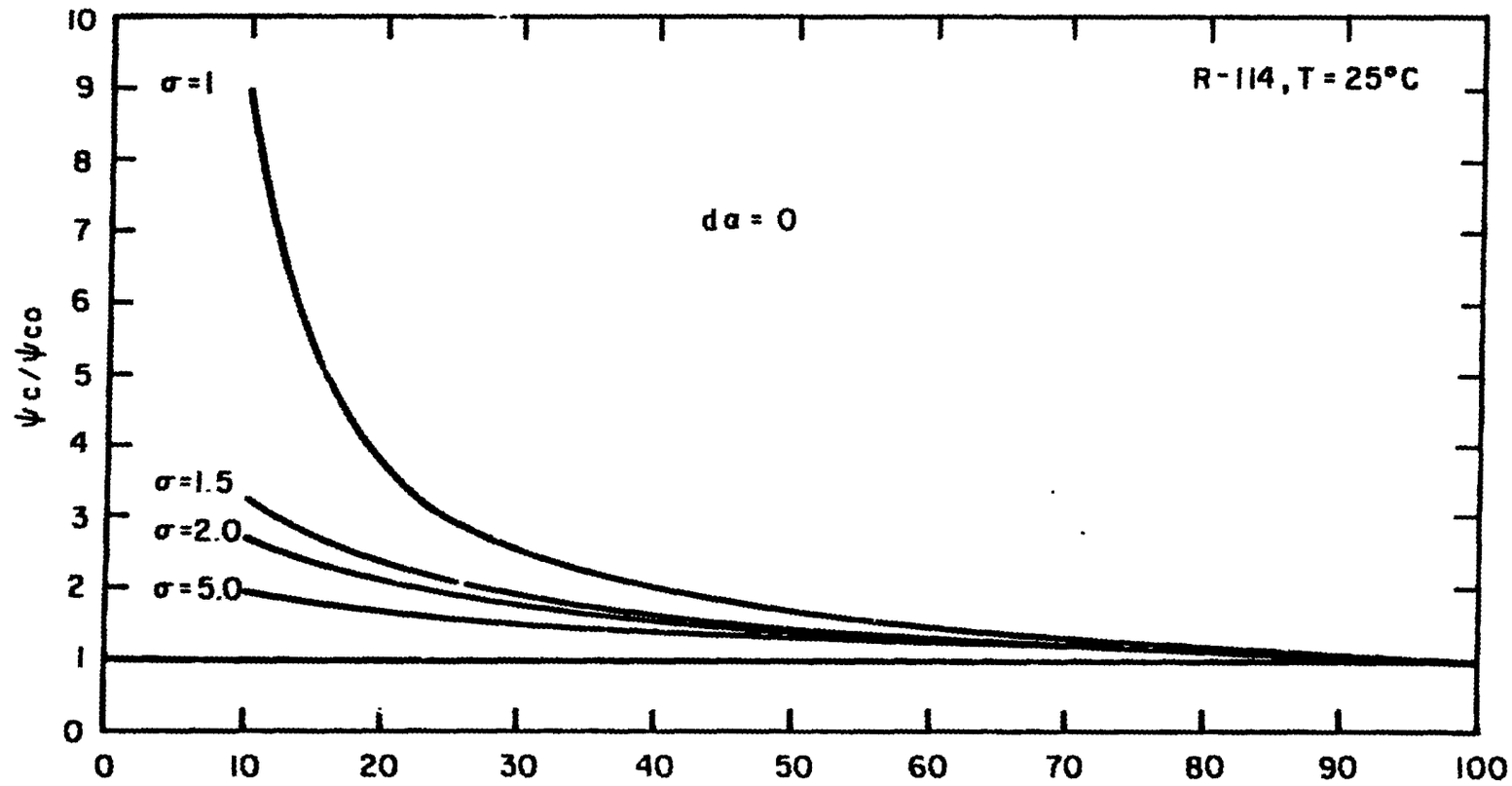
10
9
8
7
6
5
4
3
2
1
0
ψc/ψco
σ=1
σ=1.5
σ=2.0
σ=5.0
dα = 0
R-114, T = 25°C
0
10
20
30
40
50
60
70
80
90
100
x (%)

FIGURE 6

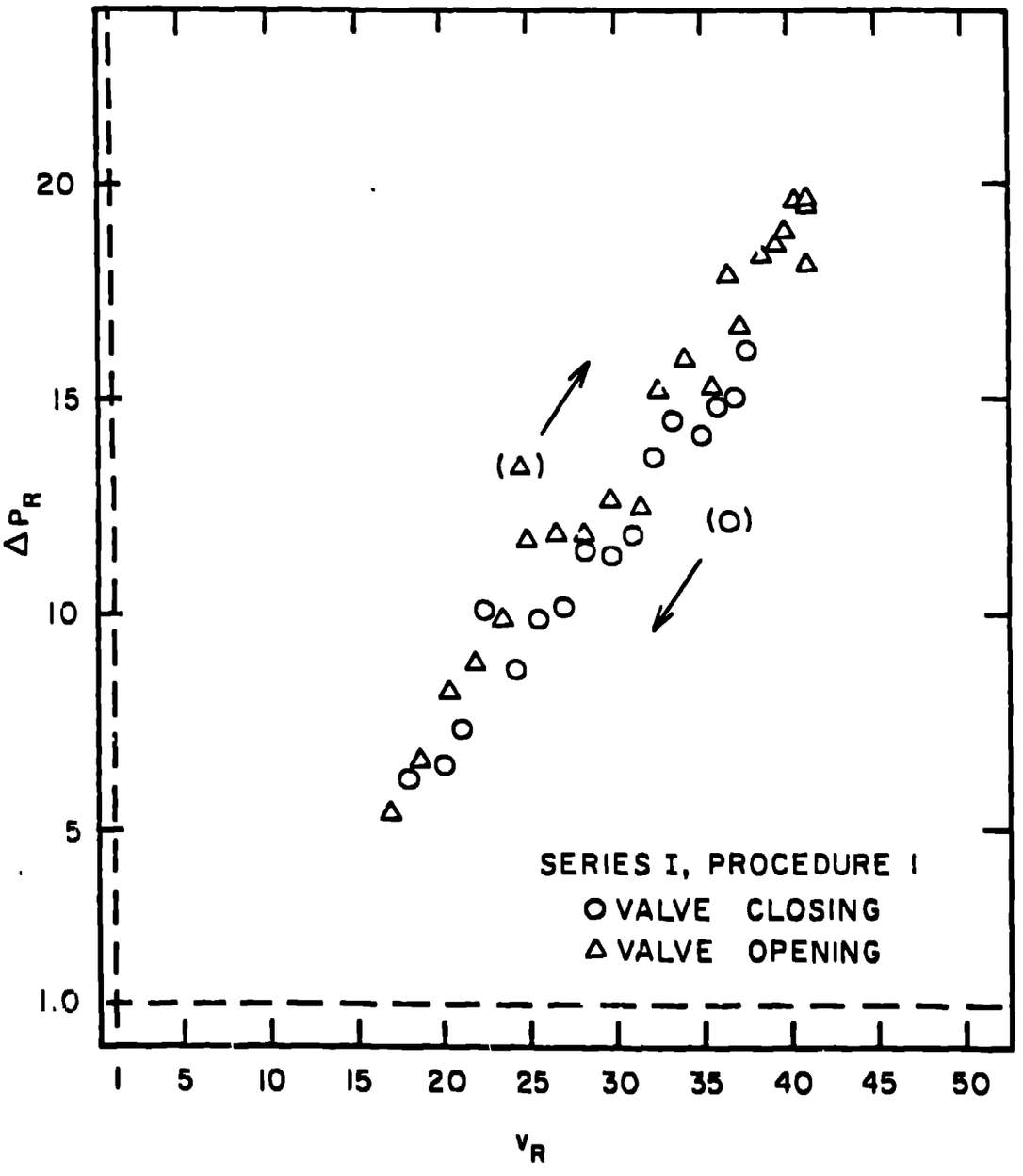
20
15
10
5
1.0
ΔP_R
(Δ)
(O)
SERIES I, PROCEDURE I
O VALVE CLOSING
Δ VALVE OPENING
1
5
10
15
20
25
30
35
40
45
50
V_R

FIGURE 7

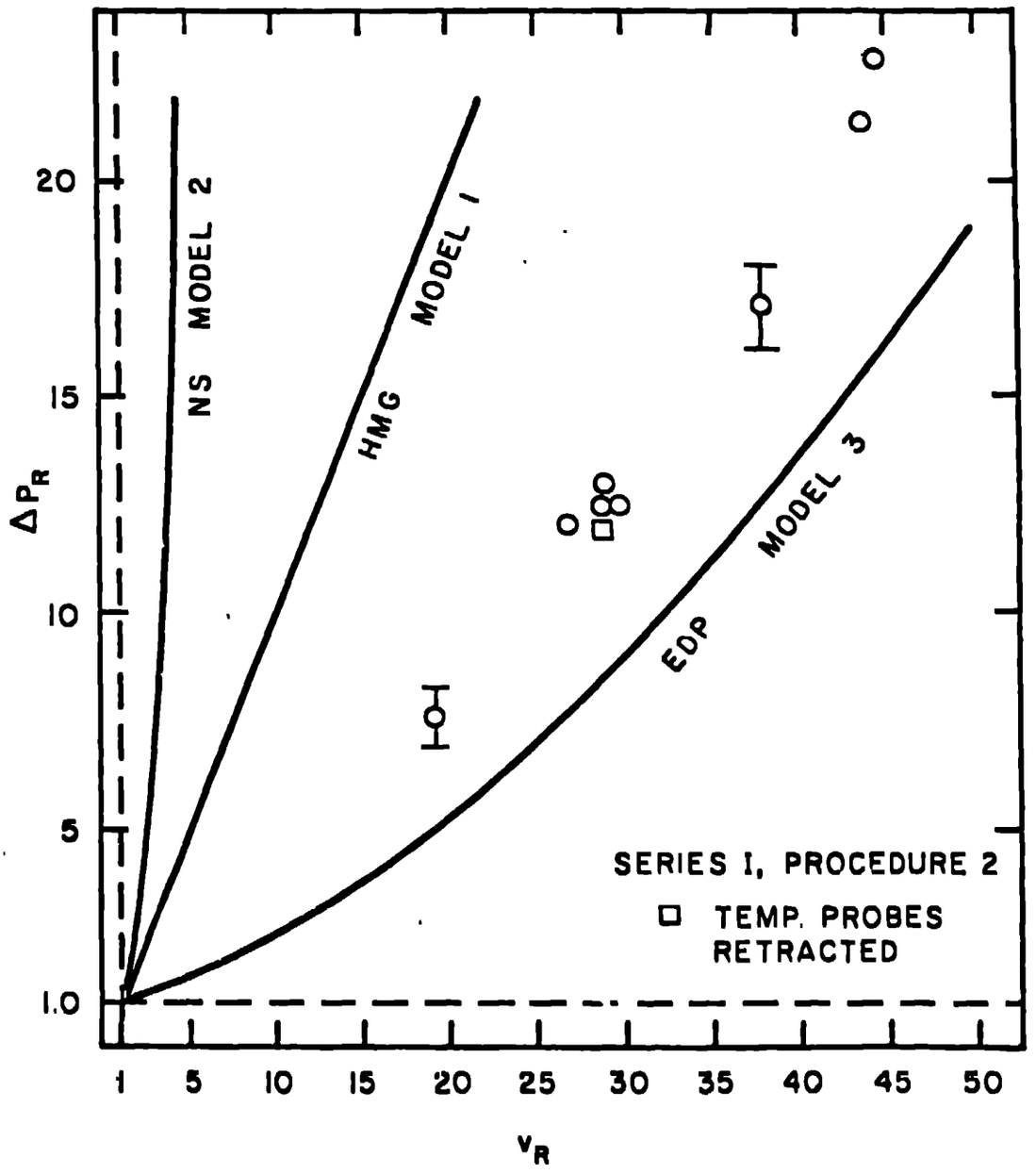
NS MODEL 2
HMG MODEL 1
EDP MODEL 3
SERIES I, PROCEDURE 2
TEMP. PROBES RETRACTED
ΔP_R
V_R
1.0
5
10
15
20
1
5
10
15
20
25
30
35
40
45
50

FIGURE 8

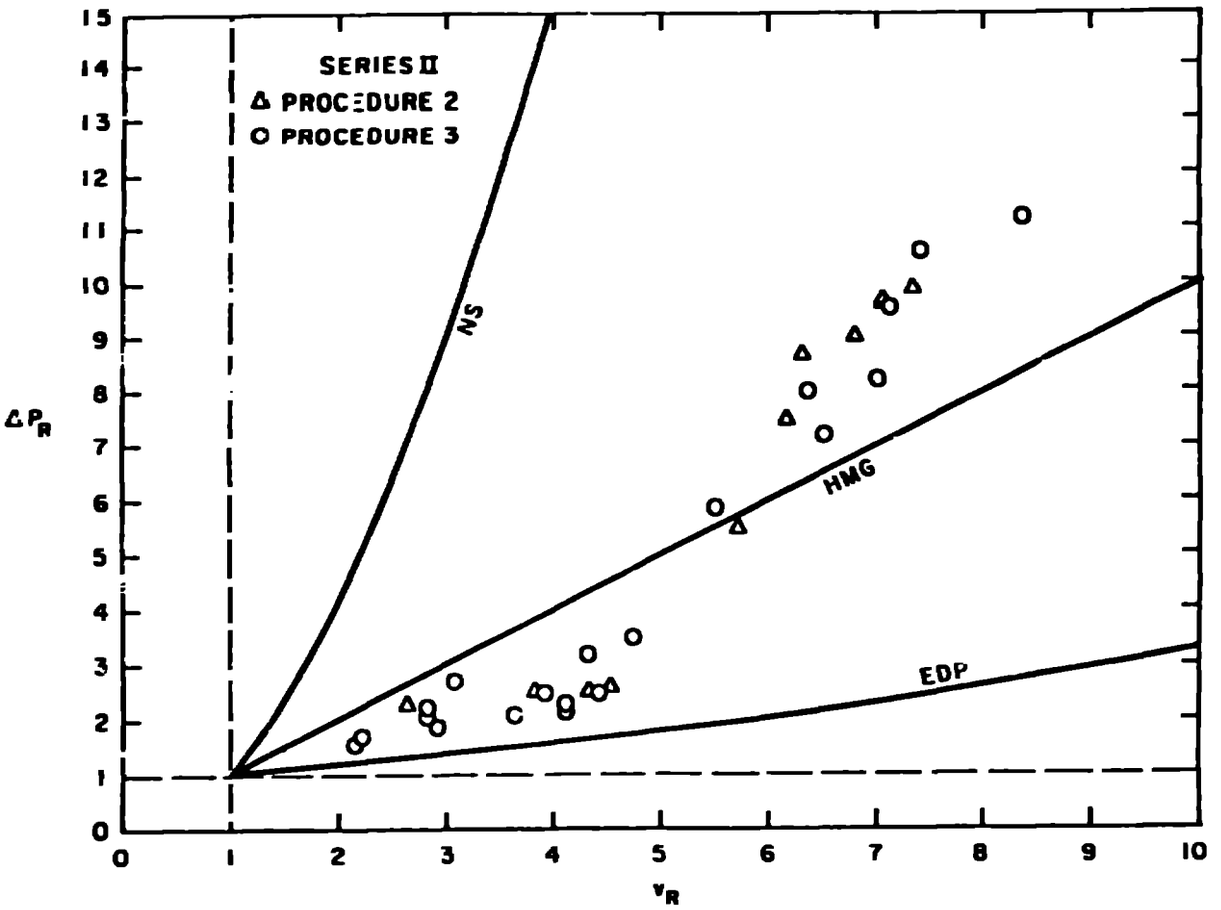
SERIES II
Δ PROCEDURE 2
O PROCEDURE 3
NS
HMG
EDP
ΔP_R
v_R
0
1
2
3
4
5
6
7
8
9
10
11
12
13
14
15

FIGURE 9

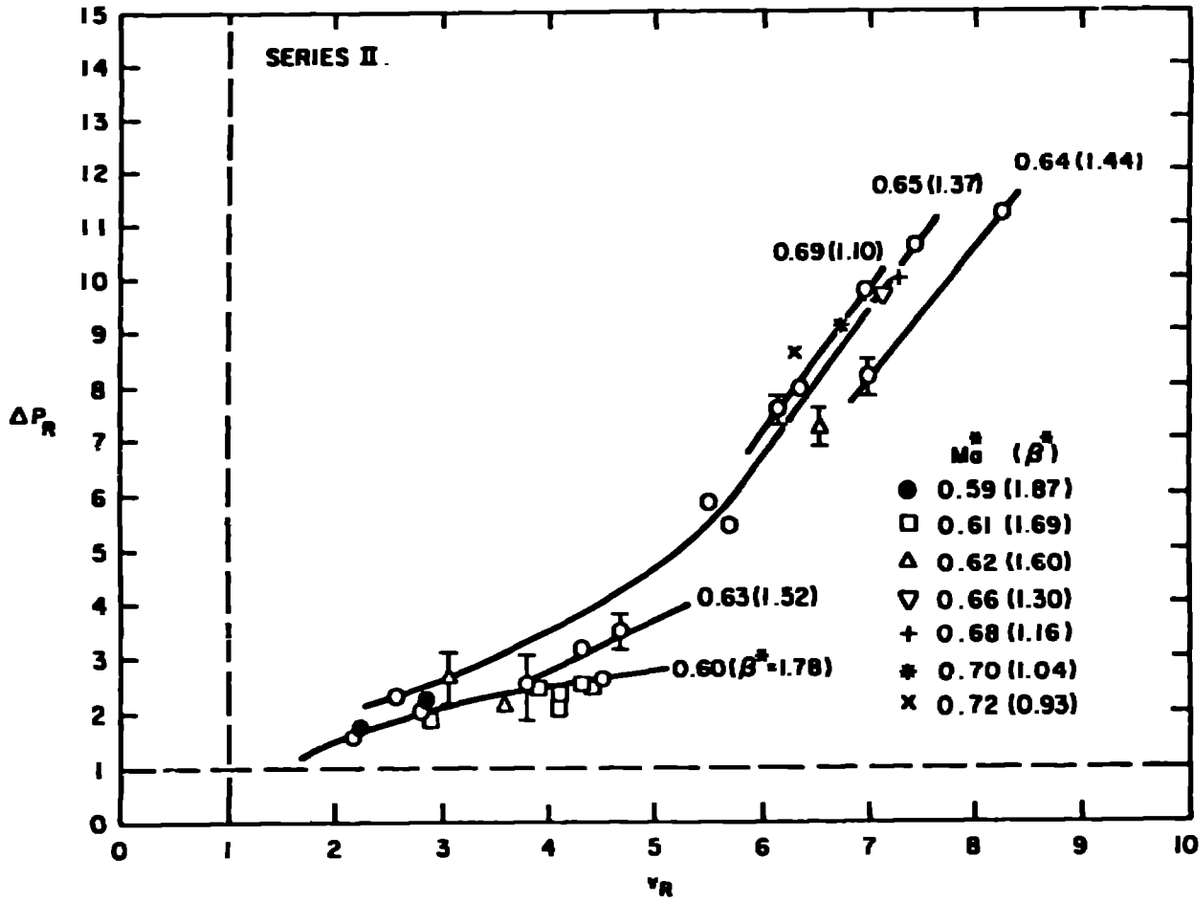
SERIES II
0.64 (1.44)
0.65 (1.37)
0.69 (1.10)
0.63 (1.52)
0.60 (β^*=1.78)
M_G^* (β^*)
0.59 (1.87)
0.61 (1.69)
0.62 (1.60)
0.66 (1.30)
0.68 (1.16)
0.70 (1.04)
0.72 (0.93)
ΔP_R
v_R

FIGURE 10

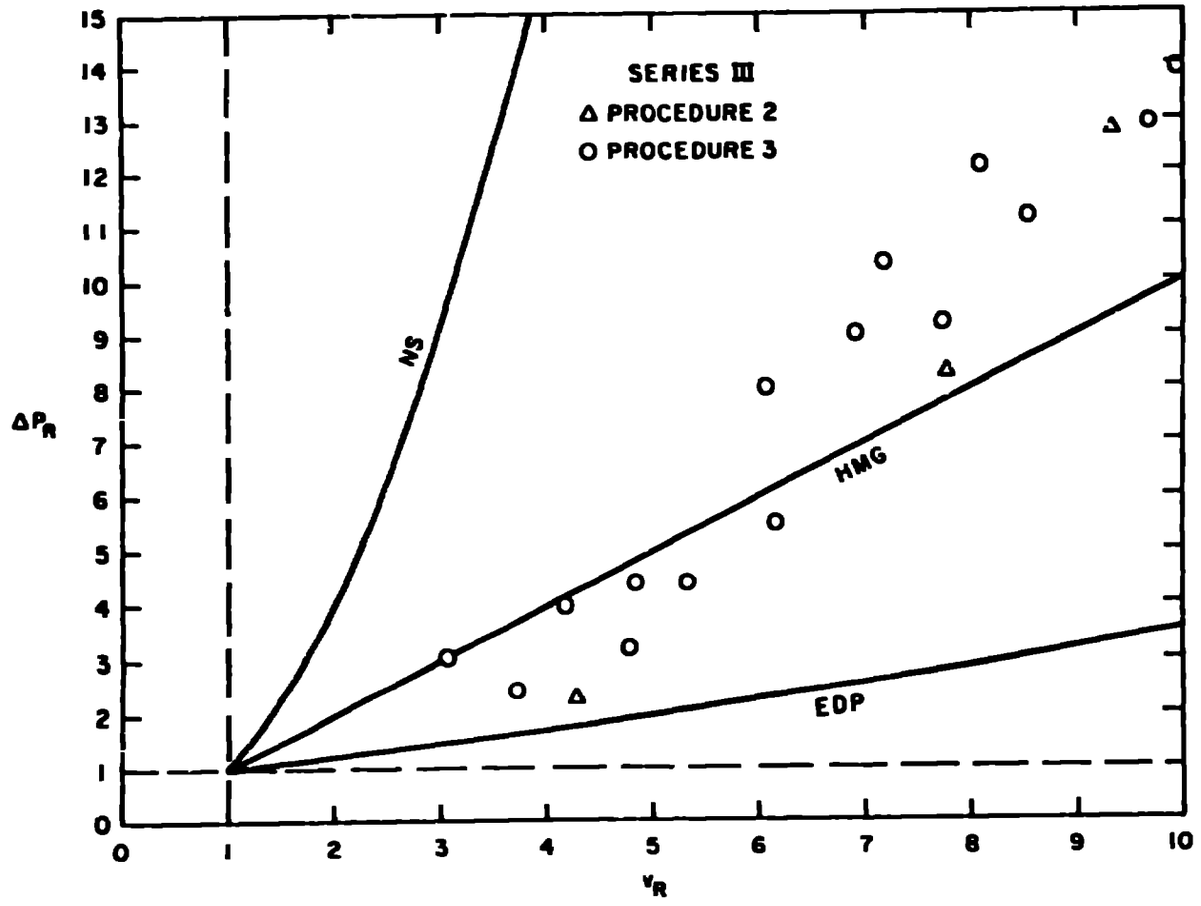
SERIES III
Δ PROCEDURE 2
O PROCEDURE 3
NS
HMG
EDP
ΔP_R
v_R
0
1
2
3
4
5
6
7
8
9
10
11
12
13
14
15

FIGURE 11

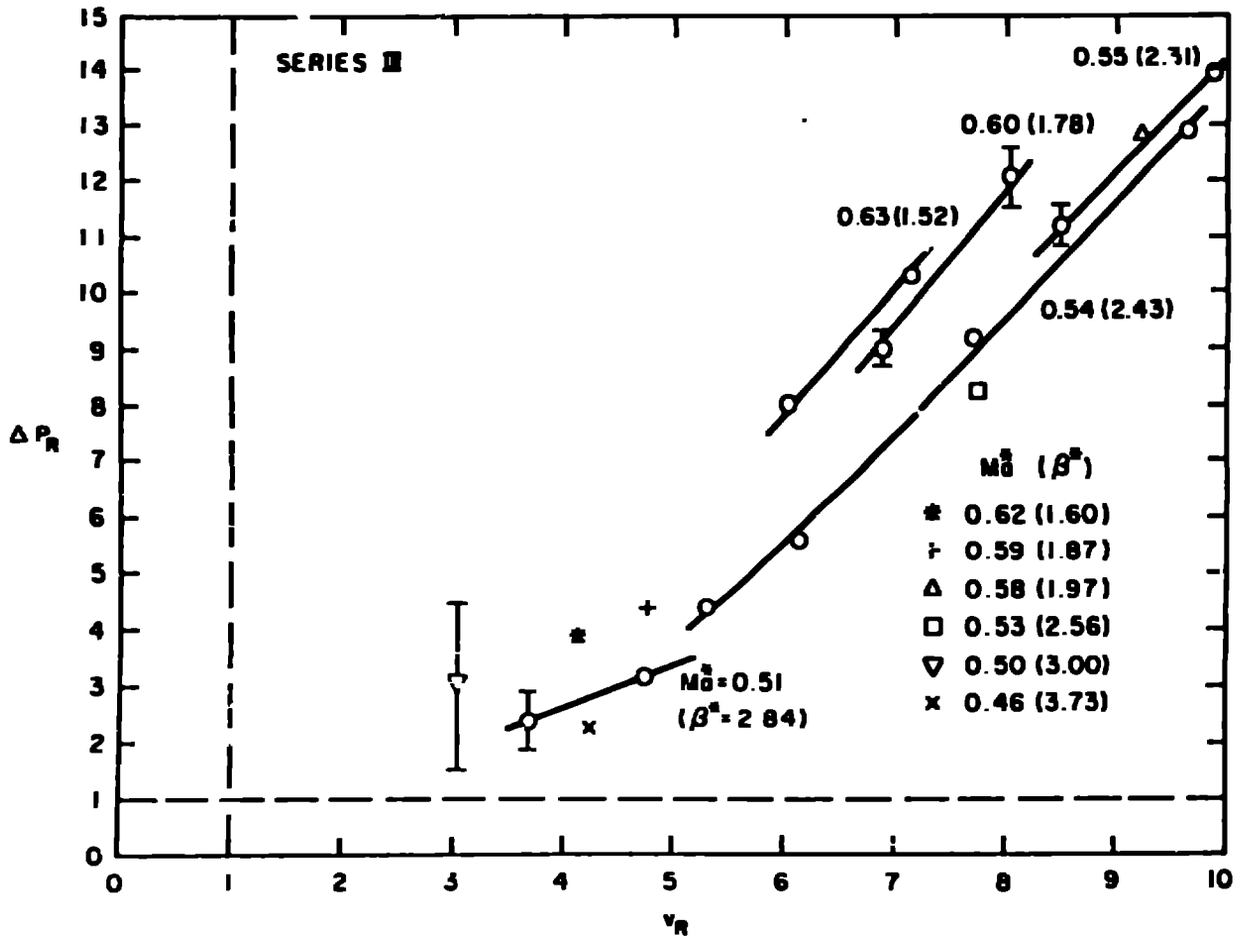
SERIES III
0.55 (2.31)
0.60 (1.78)
0.63 (1.52)
0.54 (2.43)
M_a^s (β^*)
0.62 (1.60)
0.59 (1.87)
0.58 (1.97)
0.53 (2.56)
0.50 (3.00)
0.46 (3.73)
M_a^s = 0.51
(β^* = 2.84)
ΔP_R
ν_R

FIGURE 12

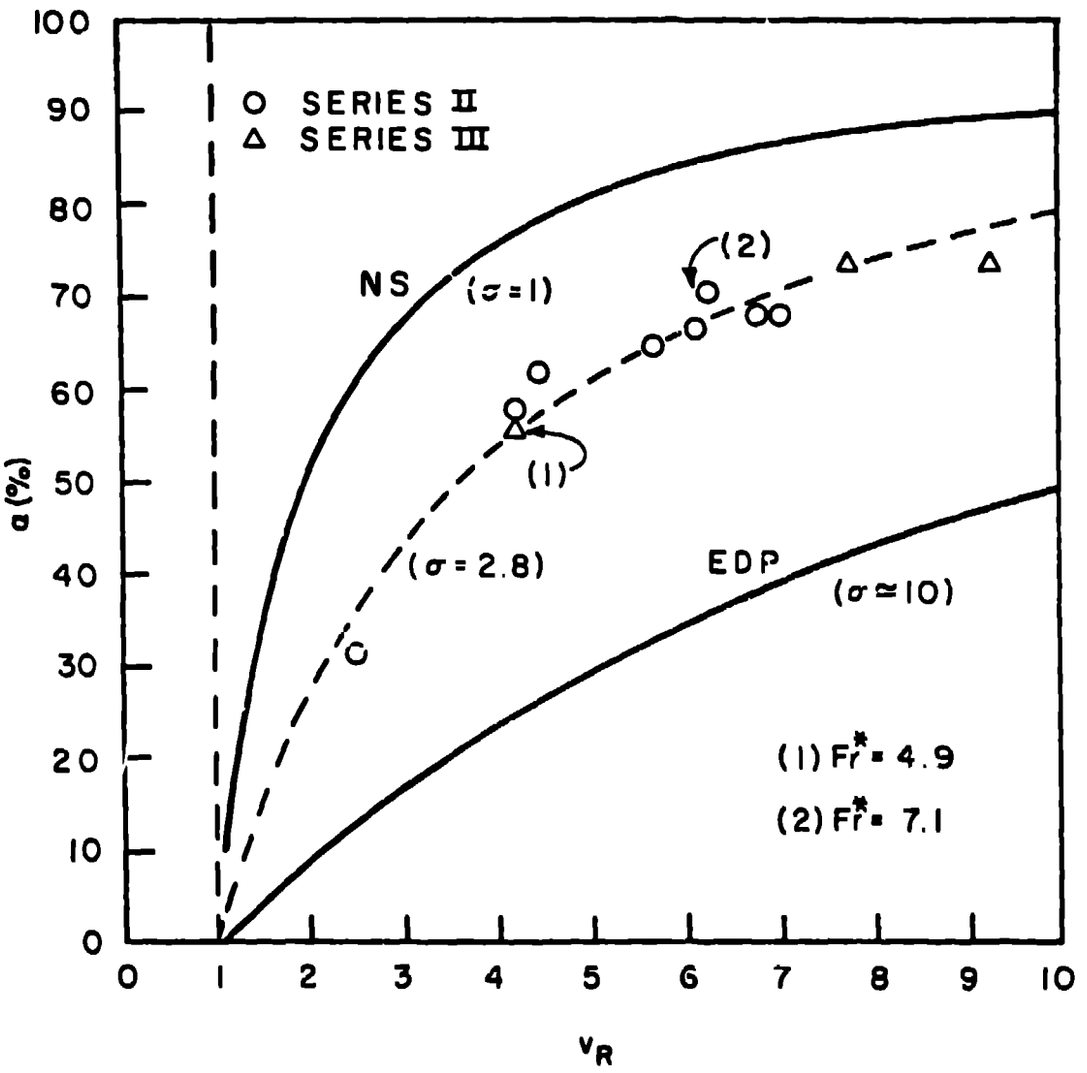
100
90
80
70
60
50
40
30
20
10
0
a (%)
O SERIES II
Δ SERIES III
NS (σ=1)
(2)
(1)
(σ = 2.8)
EDP
(σ≃10)
(1) Fr* = 4.9
(2) Fr* = 7.1
0 1 2 3 4 5 6 7 8 9 10
VR

FIGURE 13

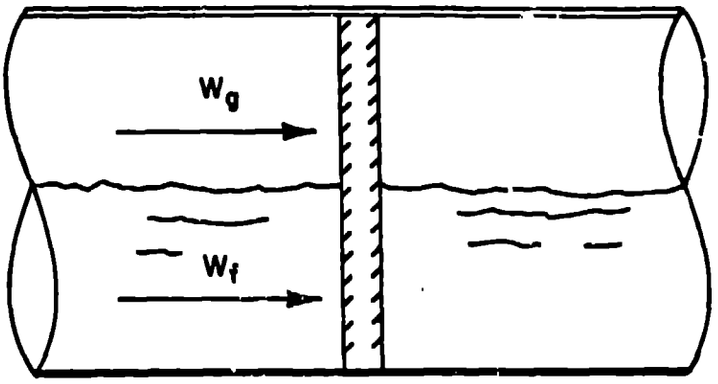

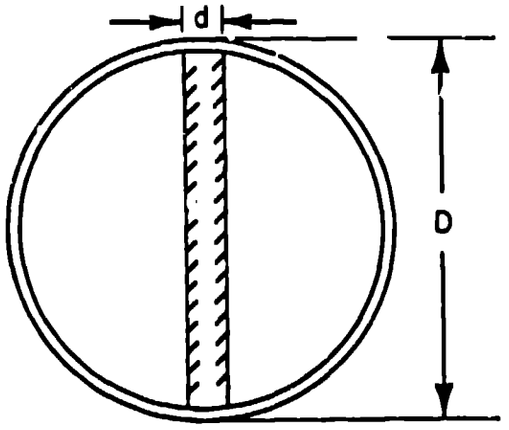

FIGURE 14

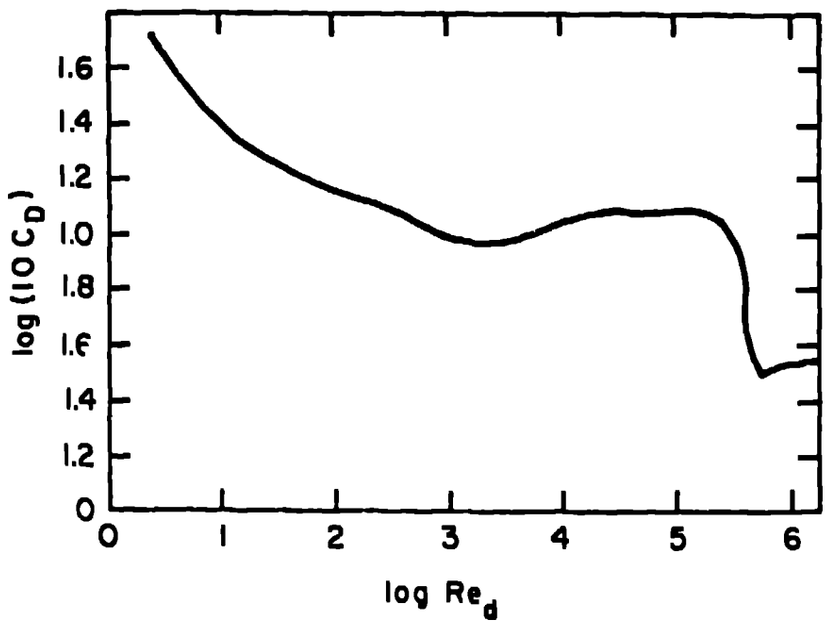

FIGURE 15

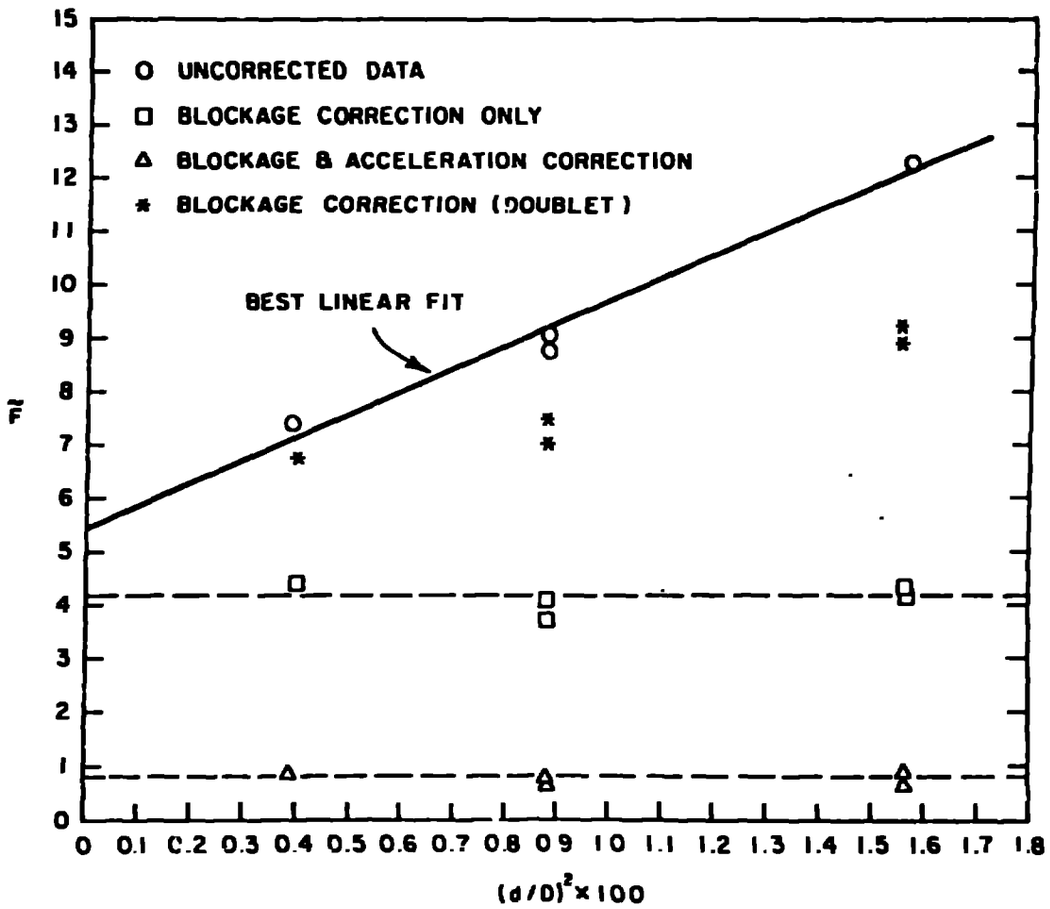
O UNCORRECTED DATA
□ BLOCKAGE CORRECTION ONLY
△ BLOCKAGE & ACCELERATION CORRECTION
* BLOCKAGE CORRECTION (DOUBLET)
BEST LINEAR FIT
$\bar{n}$
$(d/D)^2 \times 100$
0 0.1 0.2 0.3 0.4 0.5 0.6 0.7 0.8 0.9 1.0 1.1 1.2 1.3 1.4 1.5 1.6 1.7 1.8
0 1 2 3 4 5 6 7 8 9 10 11 12 13 14 15

FIGURE 16

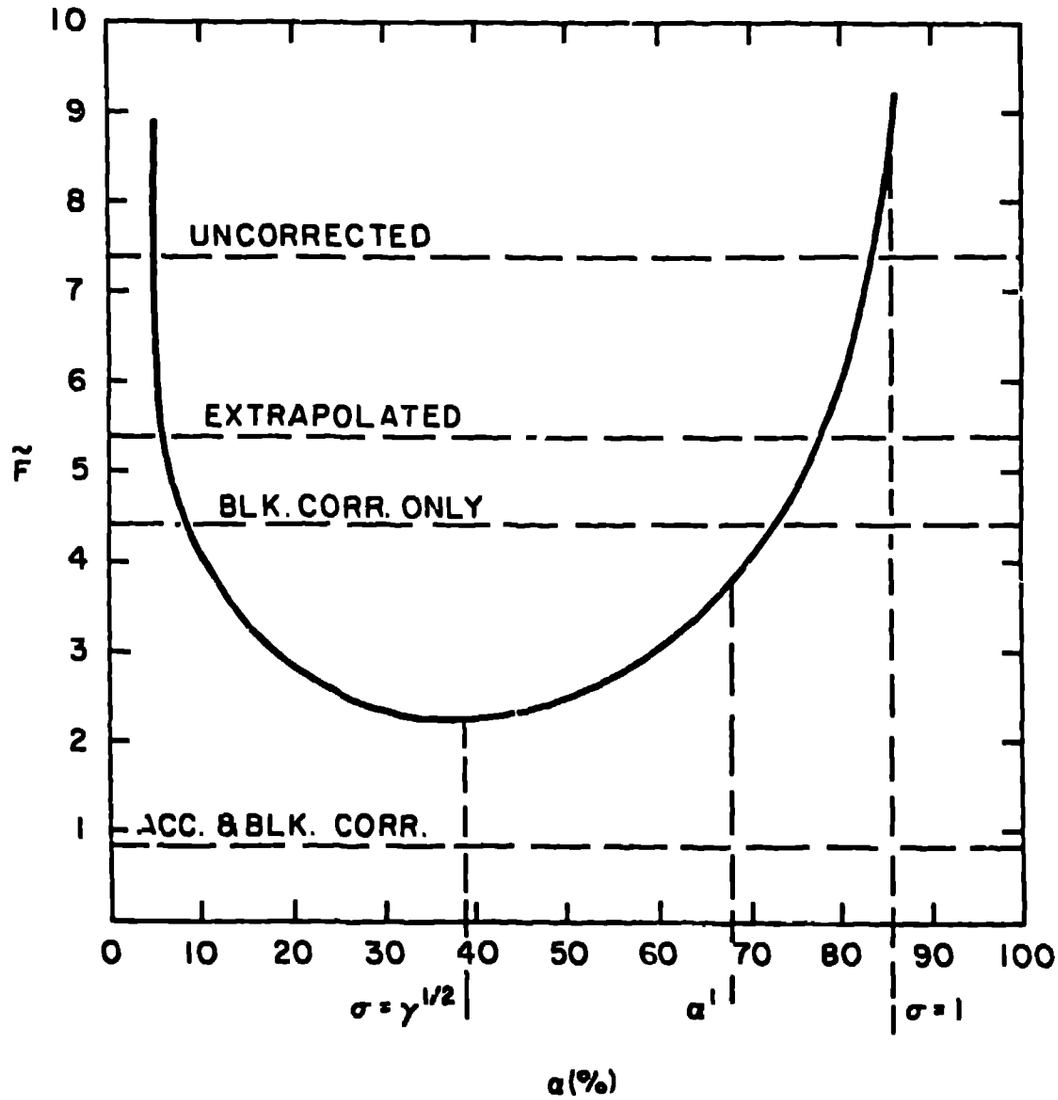
10
9
8
7
6
5
4
3
2
1
F̃
UNCORRECTED
EXTRAPOLATED
BLK. CORR. ONLY
ACC. & BLK. CORR.
0
10
20
30
40
50
60
70
80
90
100
σ = γ^1/2
α'
σ = 1
α(%)

FIGURE 17

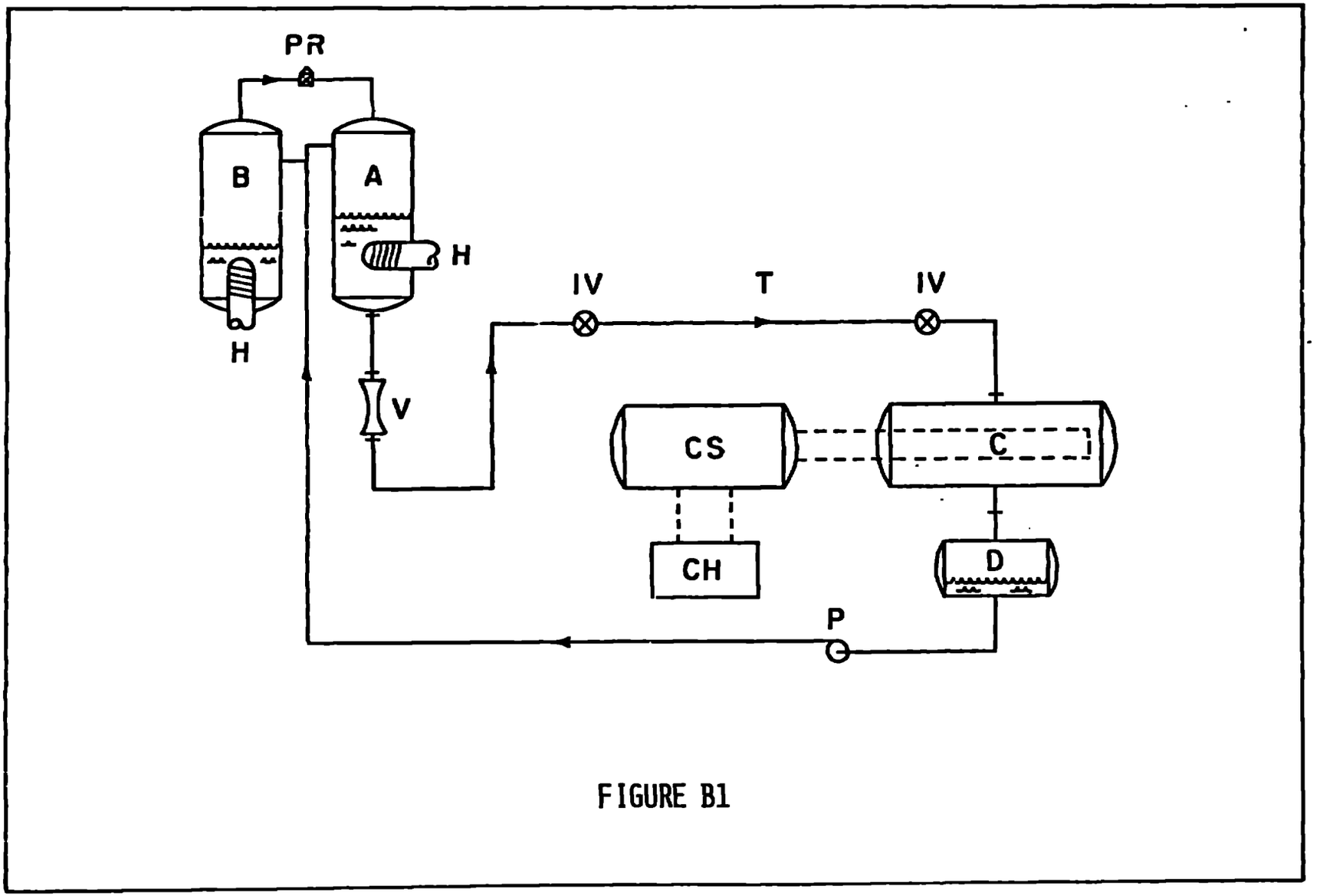

FIGURE B1

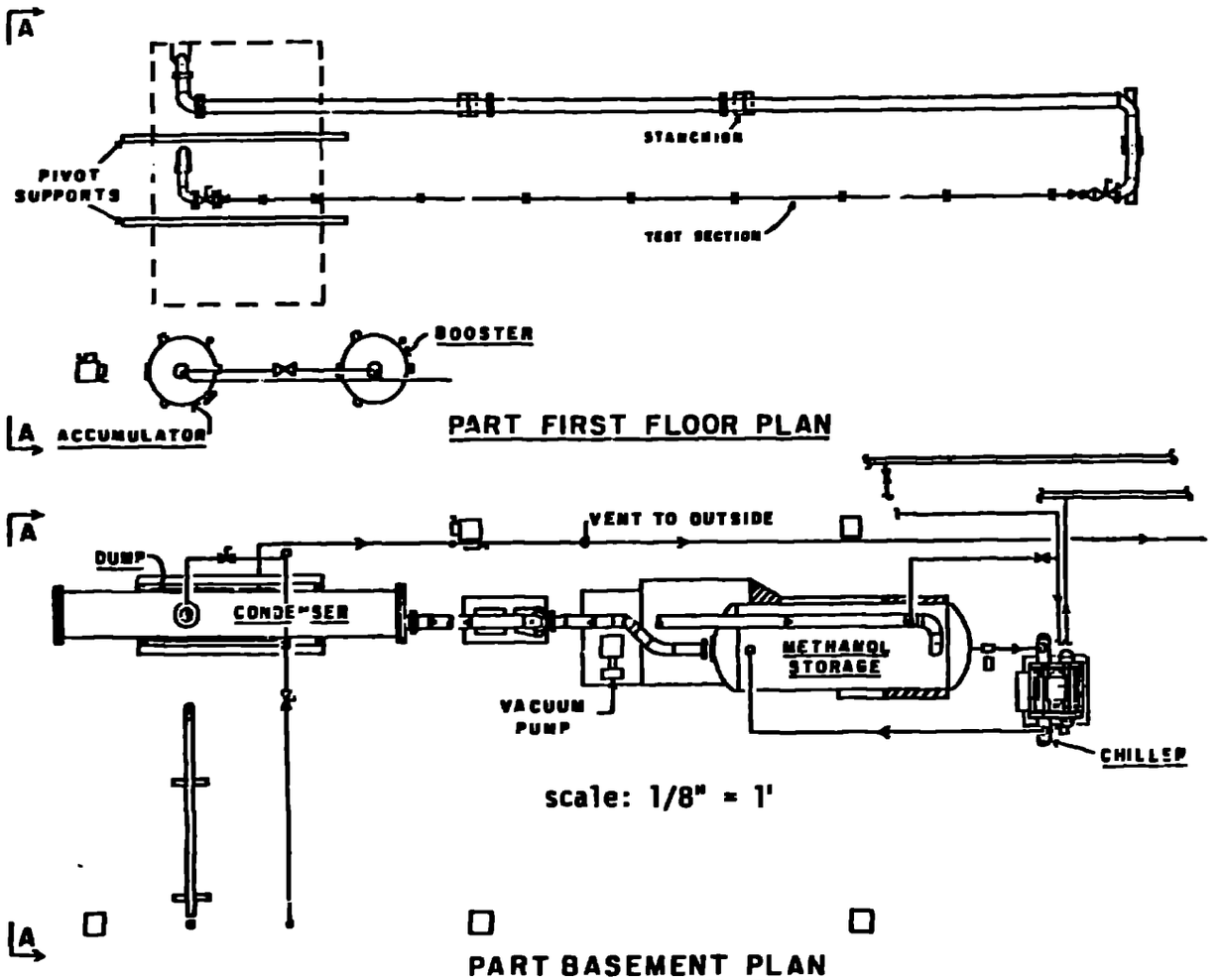
A
STANCHION
PIVOT SUPPORTS
TEST SECTION
BOOSTER
A
ACCUMULATOR
PART FIRST FLOOR PLAN
A
VENT TO OUTSIDE
DUMP
CONDENSER
METHANOL STORAGE
VACUUM PUMP
CHILLER
scale: 1/8" = 1'
A
PART BASEMENT PLAN

FIGURE B2(a)

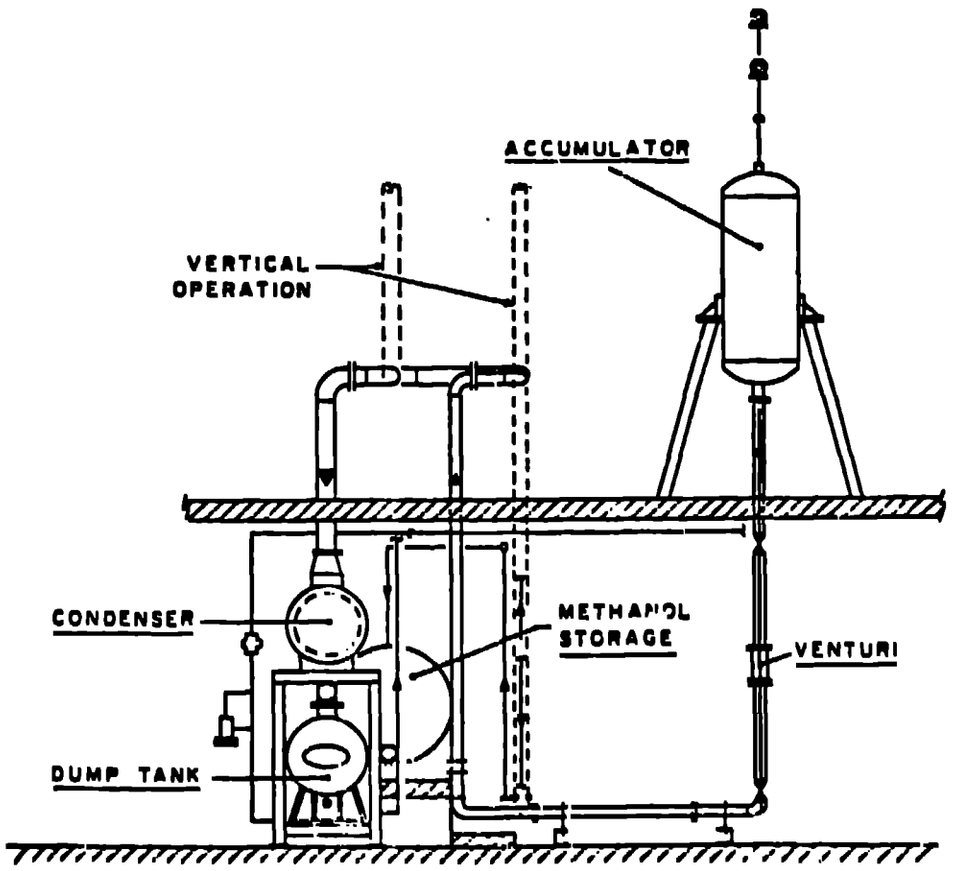

SECTION A-A

FIGURE B2(b)

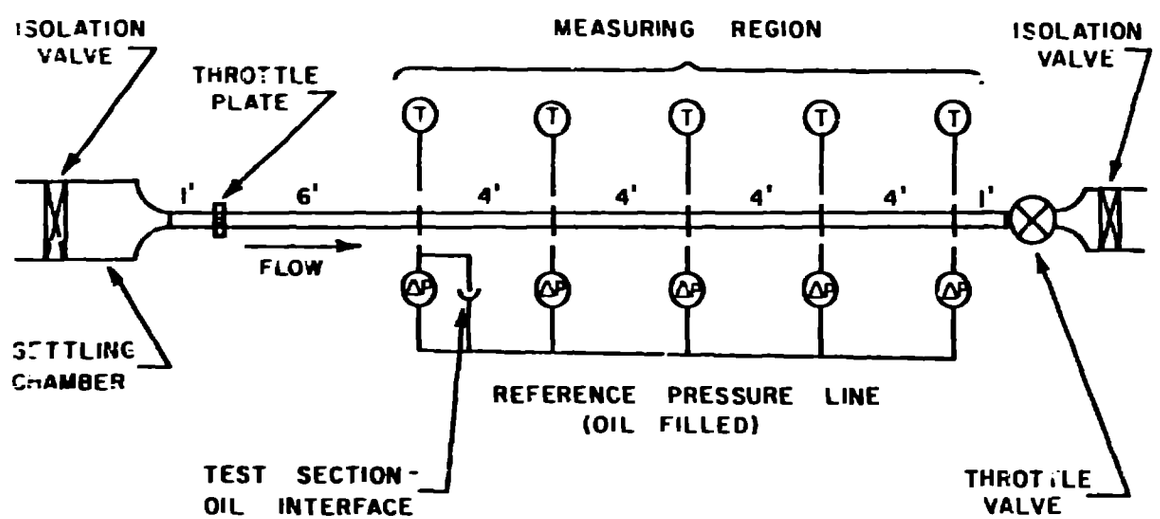
ISOLATION VALVE
THROTTLE PLATE
MEASURING REGION
ISOLATION VALVE
T
1'
6'
4'
4'
4'
4'
1'
FLOW
ΔP
SETTLING CHAMBER
REFERENCE PRESSURE LINE (OIL FILLED)
TEST SECTION - OIL INTERFACE
THROTTLE VALVE

FIGURE B3

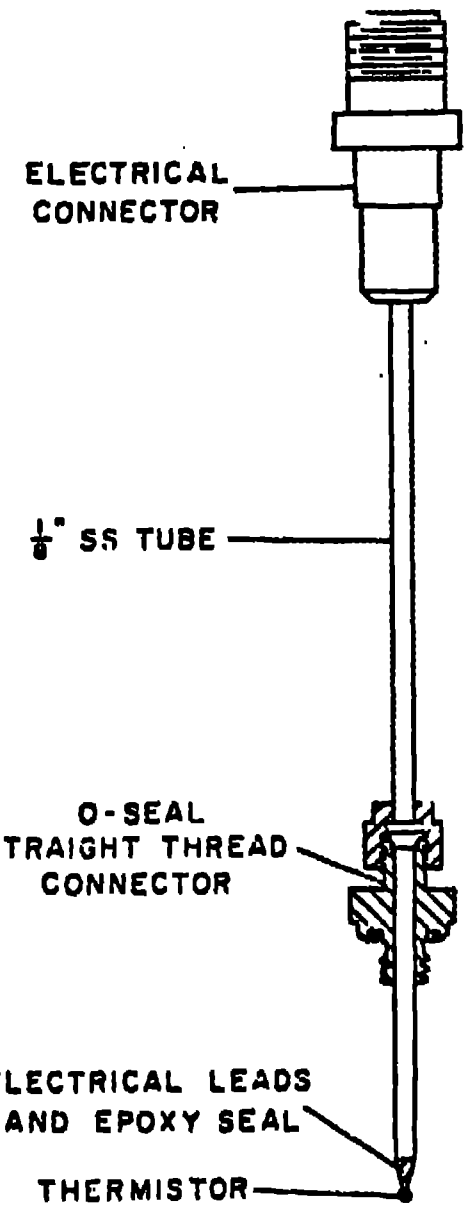

scale: 3/4

FIGURE B4

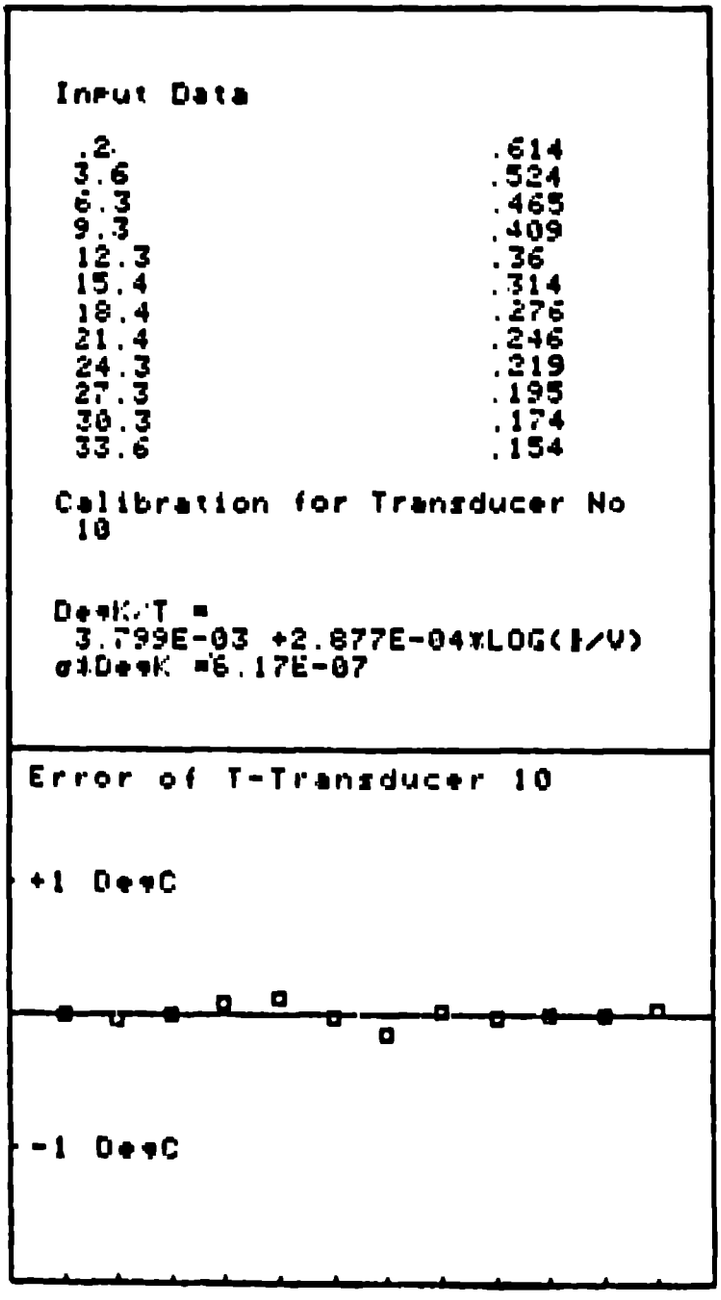
Input Data
.2 .614
3.6 .524
6.3 .465
9.3 .409
12.3 .36
15.4 .314
18.4 .276
21.4 .246
24.3 .219
27.3 .195
30.3 .174
33.6 .154
Calibration for Transducer No
10
Deg K/T =
3.799E-03 +2.877E-04*LOG(R/V)
σ1Deg K =6.17E-07
Error of T-Transducer 10
+1 Deg C
-1 Deg C

FIGURE B5

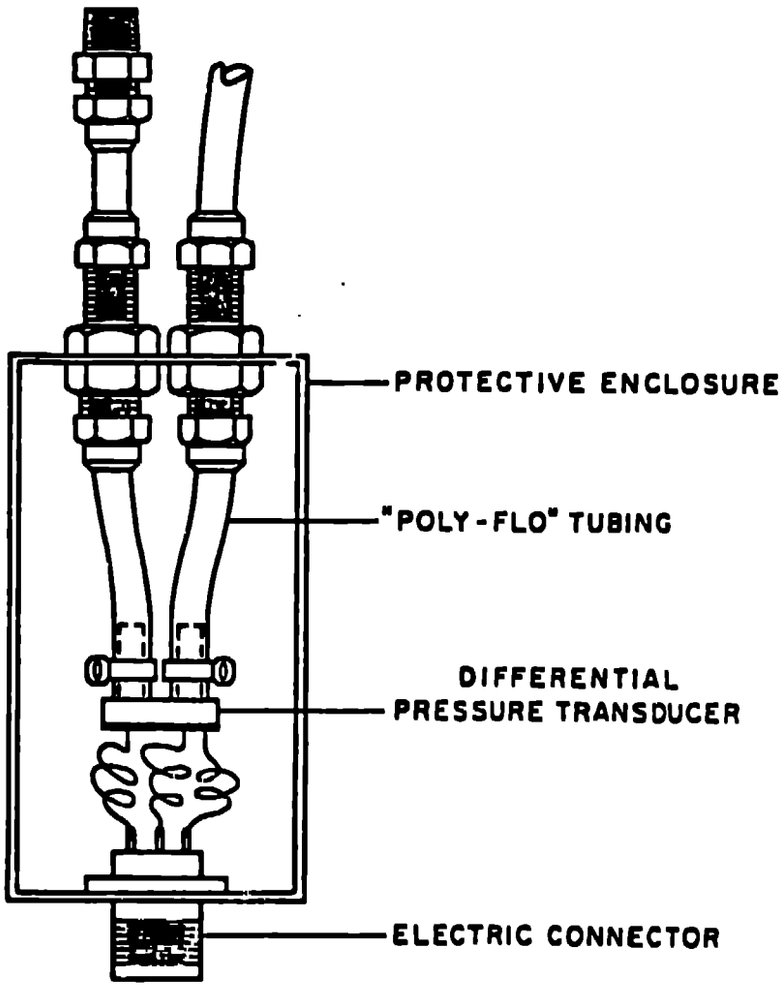

scale: 3/4

FIGURE B6

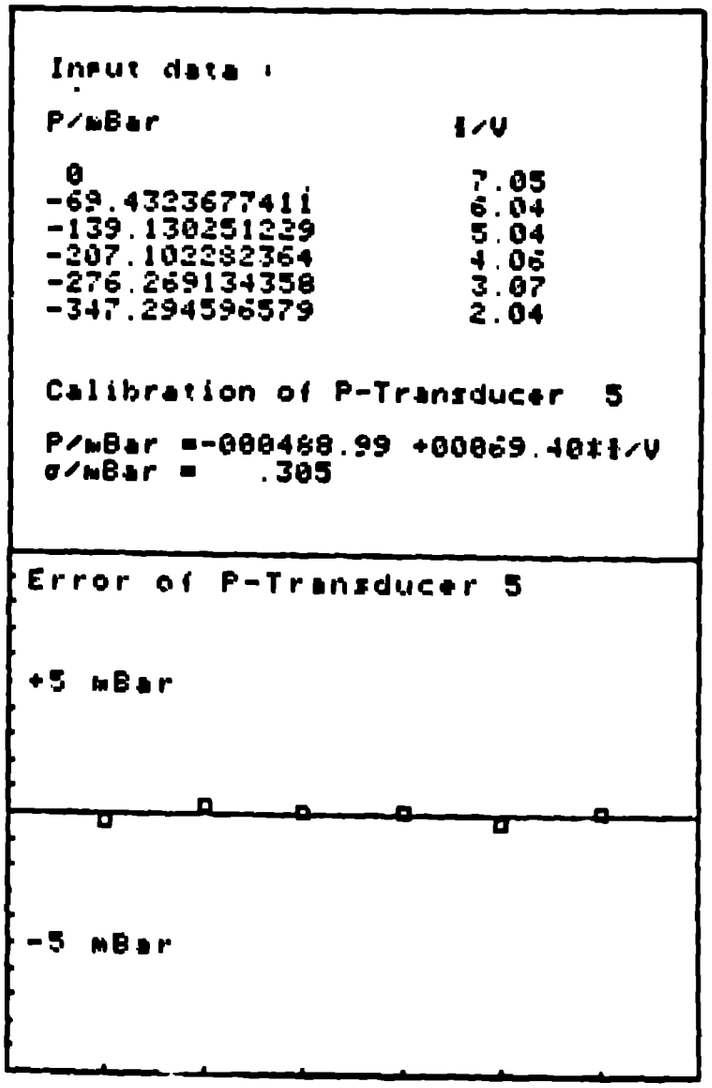
Input data :
P/mBar
I/V
0
7.05
-69.4323677411
6.04
-139.130251239
5.04
-207.102282364
4.06
-276.269134358
3.07
-347.294596579
2.04
Calibration of P-Transducer 5
P/mBar =-000468.99 +00069.40*I/V
σ/mBar = .305
Error of P-Transducer 5
+5 mBar
-5 mBar

FIGURE B7

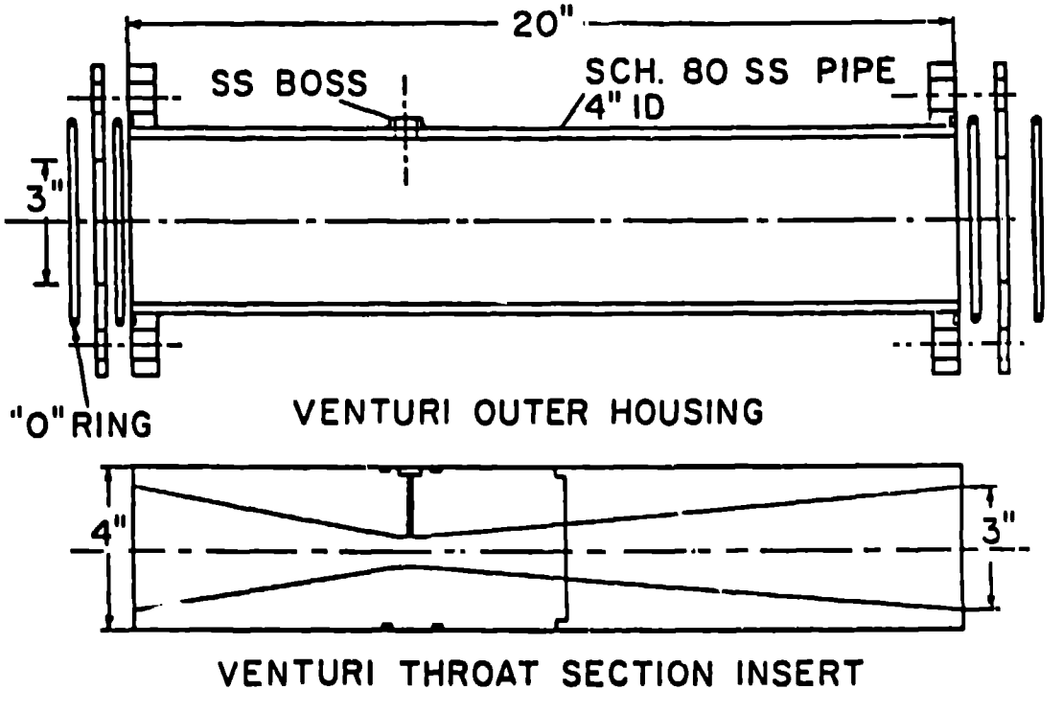
20"
SS BOSS
SCH. 80 SS PIPE
4" ID
3"
"O" RING
VENTURI OUTER HOUSING
4"
3"
VENTURI THROAT SECTION INSERT

FIGURE B8

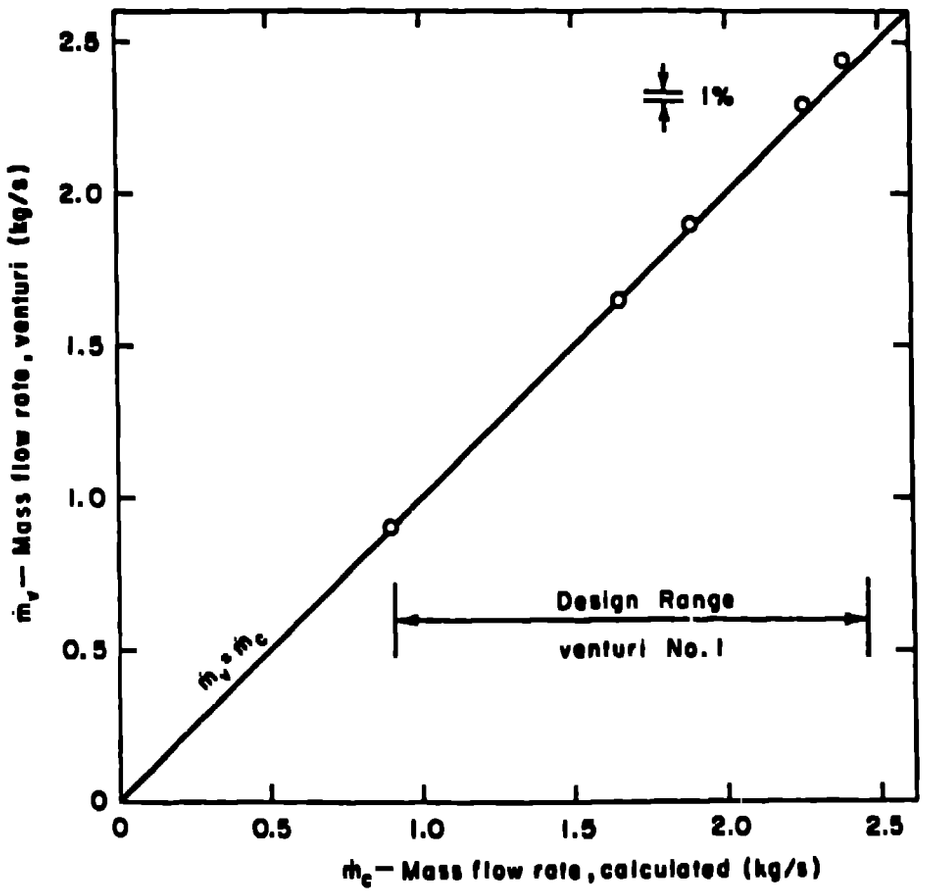
2.5
2.0
1.5
1.0
0.5
0
0
0.5
1.0
1.5
2.0
2.5
1%
Design Range
venturi No. 1
$\dot{m}_v = \dot{m}_c$
$\dot{m}_v$ — Mass flow rate, venturi (kg/s)
$\dot{m}_c$ — Mass flow rate, calculated (kg/s)

FIGURE B9(a)

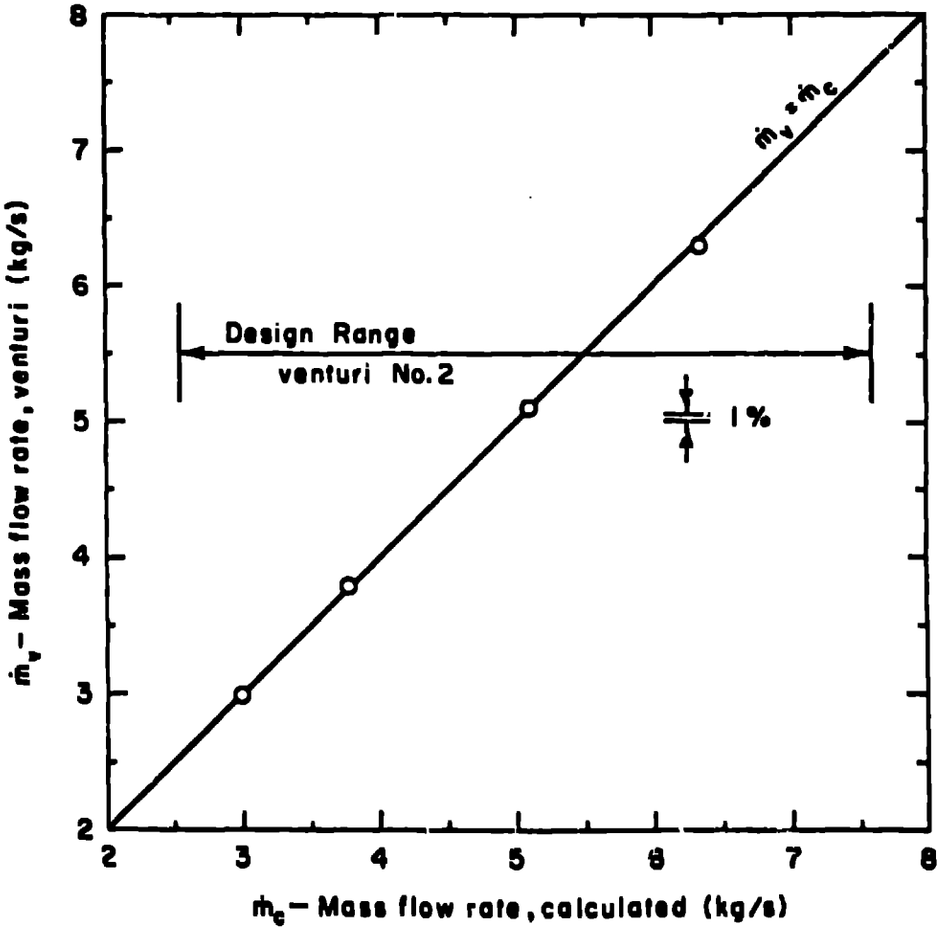
8
7
6
5
4
3
2
2
3
4
5
6
7
8
$\dot{m}_v = \dot{m}_c$
Design Range
venturi No. 2
1%
$\dot{m}_v$ – Mass flow rate, venturi (kg/s)
$\dot{m}_c$ – Mass flow rate, calculated (kg/s)

FIGURE B9(b)

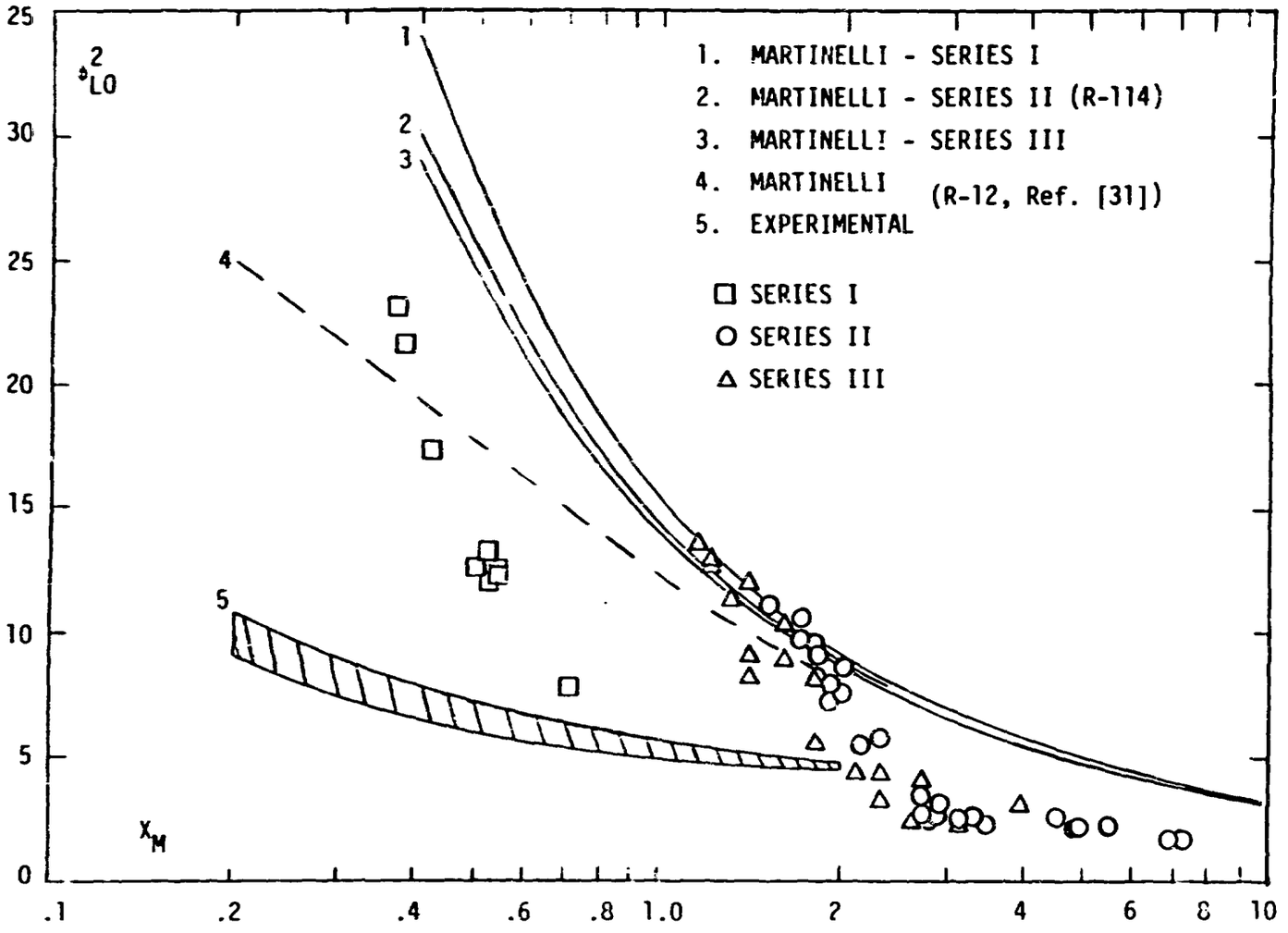
1. MARTINELLI - SERIES I
2. MARTINELLI - SERIES II (R-114)
3. MARTINELLI - SERIES III
4. MARTINELLI (R-12, Ref. [31])
5. EXPERIMENTAL
SERIES I
SERIES II
SERIES III
ϕ^2_{LO}
X_M
25
30
25
20
15
10
5
0
.1
.2
.4
.6
.8
1.0
2
4
6
8
10

FIGURE C1.

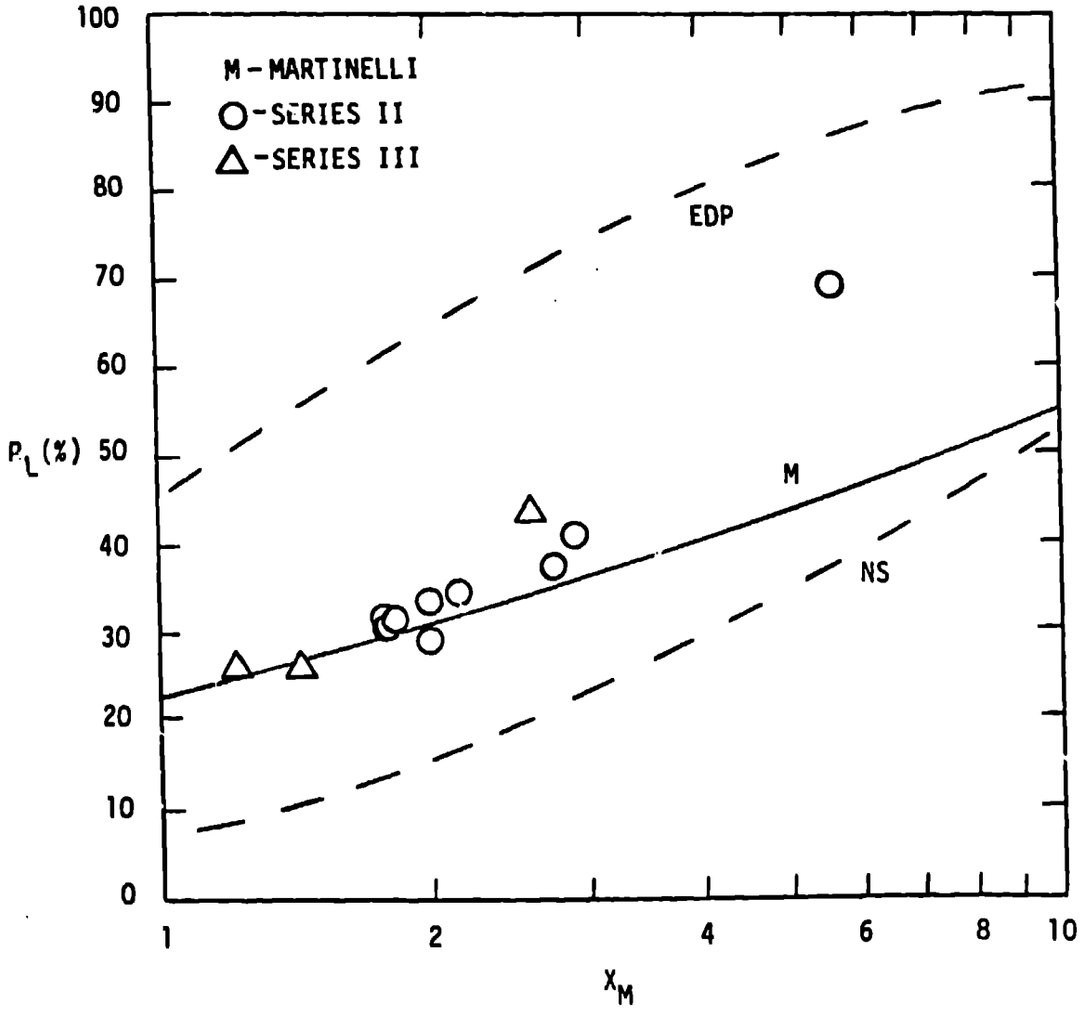
M - MARTINELLI
O - SERIES II
Δ - SERIES III
EDP
M
NS
P_L (%)
X_M
100
90
80
70
60
50
40
30
20
10
0
1
2
4
6
8
10

FIGURE C2.

TABLE 1 BASIC PARAMETERS - DATA SERIES I, II, III

	$\overline{Fr}^*$ max.	$\overline{\dot{m}}$(kg/s)	$\overline{Re}^*/10^5$	$\overline{Fr}^*$	$\overline{Ma}^*$	v_R Range
		Range	Range	Range	Range	Ma_o Range
Series I T_0 = 25°C	13	2.28	1.70	1.2	.29	19 - 45
		2.23 - 2.34	1.63 - 1.74	1.1 - 1.3	.27 - .30	.50 - .84
Series II T_0 = 25°C	13	5.00	3.72	5.8	.64	2 - 9
		4.64 - 5.53	3.45 - 4.08	5.0 - 7.1	.59 - .72	.63 - .91
Series III T_0 = 35°C	22	5.33	4.35	6.9	.56	3 - 10
		4.50 - 6.02	3.70 - 4.90	4.9 - 8.7	.46 - .63	.55 - .86

Table BI - Valve Positions, Series I

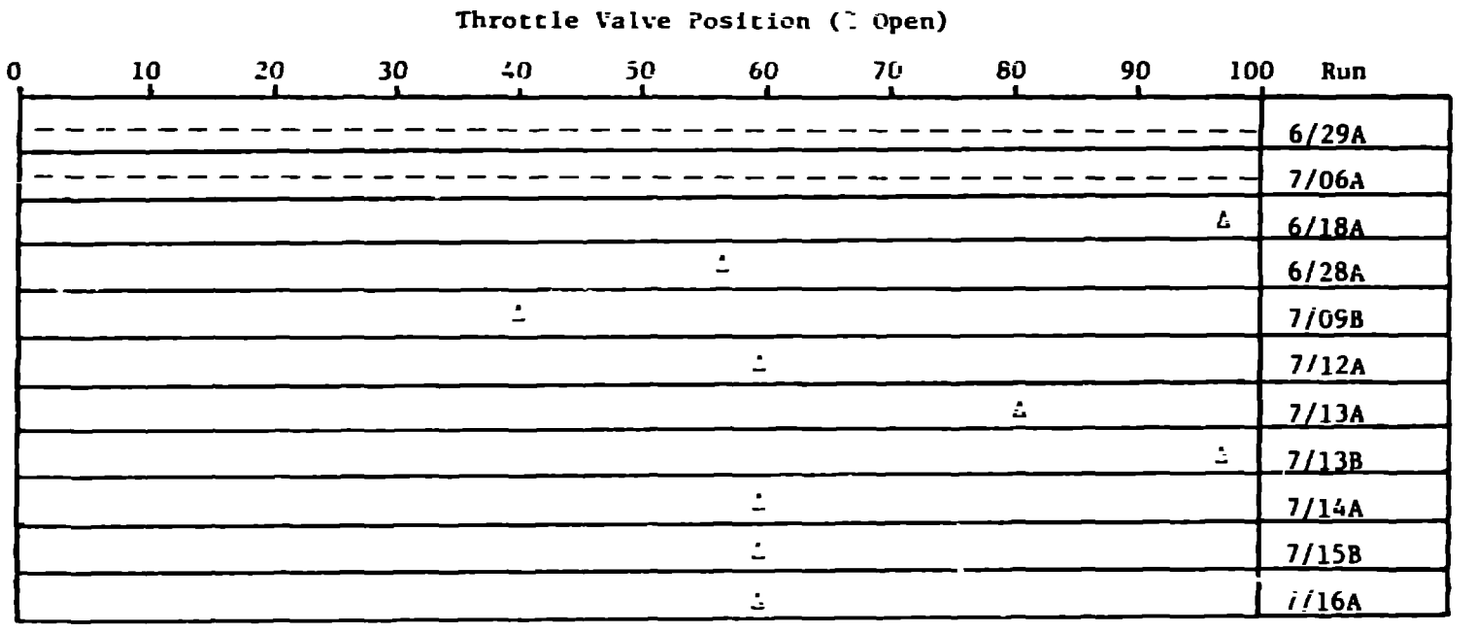

– – – Procedure 1, No Time Average

: Procedure 2, 12 Scan Time Average

Table B2 - Valve Positions, Series II

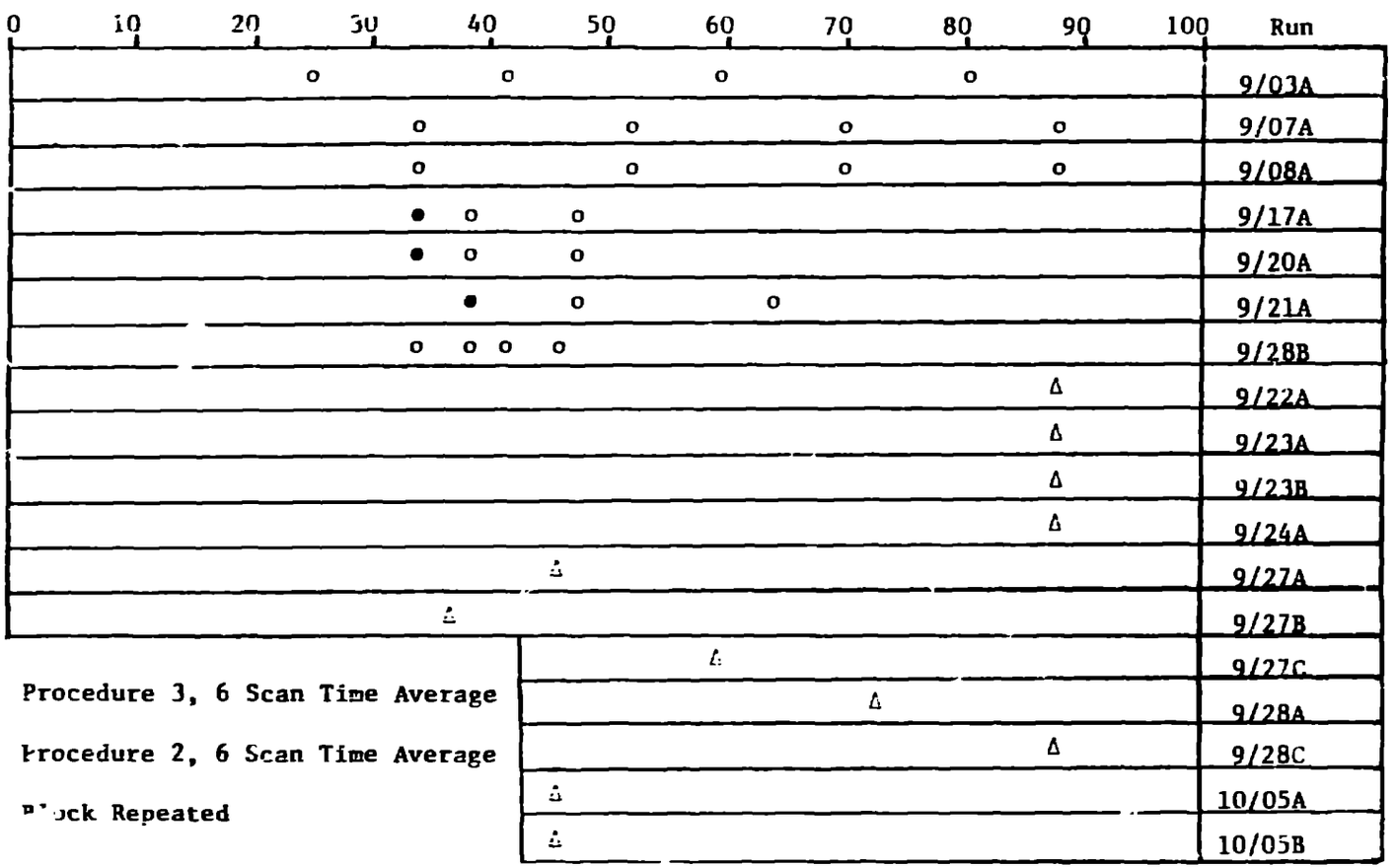

Table B3 - Valve Positions, Series III

Throttle Valve Position (% Open)

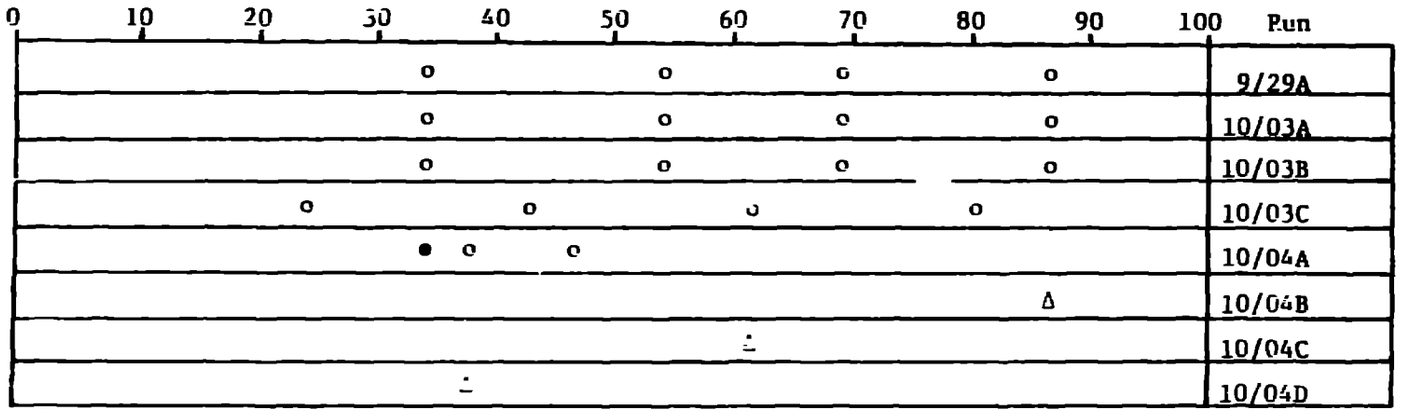

o Procedure 3, 6 Scan Time Average

± Procedure 2, 6 Scan Time Average

● Block Repeated

Table B4 - Data Series I

Run	$\dot{m}$(kg/s)	T_o(^oC)	$P_o-P_s(T_o)$ (kPa)	$Re^*/10^5$	Fr^*	Ma^*	T(^oC)	%x	v_R	M_{uc}	ΔP_R	
6/18A	2.31	27.2	86.5	1.73	1.2	.29	0.0	19.2	43.7	.84	21.5	---
6/28A	2.23	27.3	83.5	1.67	1.2	.28	6.7	15.1	27.1	.61	12.2	---
7/6B	2.16	27.8	83.8	1.63	1.1	.27	11.2	12.5	19.3	.50	7.70	---
7/12A	2.27	26.3	93.2	1.68	1.2	.29	5.3	15.2	28.7	.66	12.6	---
7/13A	2.31	26.4	94.0	1.72	1.2	.30	1.6	17.7	38.1	.78	17.2	---
7/13B	2.30	27.7	82.4	1.73	1.2	.28	0.0	19.6	44.6	.84	22.9	---
7/15A	2.27	27.3	89.0	1.71	1.2	.28	5.4	15.9	30.0	.66	12.6	---
7/15B	2.34	26.2	100.1	1	1.3	.30	5.2	15.3	29.0	.68	12.0	---
7/16A	2.29	26.0	94.8	1.6	1.2	.30	5.0	15.2	29.1	.67	13.2	---

Table B5 - Data Series II

Run	$\dot{m}$(kg/s)	T_o(^oC)	$P_o-P_s(T_c)$ (kPa)	$Re^*/10^5$	Fr^*	Ma^*	T(^oC)	%x	v_R	Ma_o	ΔP_R	α(%)
9/22A	5.31	26.5	31.6	3.95	6.5	.68	19.1	5.69	7.34	.89	9.95	---
9/23A	5.45	26.4	38.9	4.05	6.9	.70	19.5	5.27	6.77	.90	9.02	67.6
9/23B	5.38	26.3	35.7	3.99	6.7	.69	19.2	5.46	7.05	.90	9.71	67.9
9/24A	5.39	26.4	35.6	4.00	6.7	.69	19.3	5.46	7.03	.90	9.70	68.1
9/27A	4.87	27.2	29.7	3.65	5.5	.61	22.9	3.37	4.29	.71	2.55	58.5
9/27B	4.99	25.7	39.2	3.68	5.7	.65	23.7	1.66	2.58	.70	2.27	31.3
9/27C	5.12	26.9	31.8	3.83	6.1	.65	21.1	4.55	5.73	.80	5.47	64.6
9/28A	5.36	26.0	37.0	3.96	6.6	.69	19.8	4.75	6.15	.87	7.53	66.1
9/28C	5.53	25.7	41.5	4.08	7.1	.72	19.5	4.80	6.27	.91	8.69	70.9
10/05A	4.98	27.1	34.3	3.73	5.8	.63	23.4	2.93	3.81	.72	2.54	---
10/05B	4.85	27.5	28.2	3.65	5.5	.60	22.9	3.58	4.50	.71	2.61	61.8

Table B5 - Data Series II (cont.)

Run	$\dot{m}$(kg/s)	T_o(^oC)	$P_o-P_s(T_o)$ (kPa)	$Re^*/10^5$	Fr^*	Ma^*	T(^oC)	z_x	v_R	Ma_o	ΔP_R	
9/03A a												
b	4.77	25.6	31.6	3.51	5.2	.62	23.0	2.10	3.04	.69	2.73	---
c	5.02	25.8	29.1	3.71	5.8	.65	20.4	4.20	5.47	.80	5.86	---
d	5.07	25.9	26.6	3.75	5.9	.66	18.8	5.44	7.11	.86	9.56	---
9/07A a												
b	4.94	26.4	30.4	3.67	5.6	.63	22.2	3.31	4.31	.74	3.19	---
c	5.09	26.5	28.6	3.79	6.0	.65	20.0	4.97	6.34	.83	8.00	---
d	5.11	26.5	26.4	3.80	6.0	.65	19.0	5.77	7.43	.86	10.62	---
9/08A a												
b	4.94	26.6	29.9	3.68	5.7	.63	22.0	3.64	4.66	.75	3.50	---
c	5.09	26.8	26.7	3.80	6.0	.64	19.7	5.53	7.03	.84	8.24	---
d	5.08	26.9	23.9	3.80	6.0	.64	18.5	6.48	8.36	.88	11.19	---

Table B5 - Data Series II (cont.)

	$\dot{m}$(kg/s)	T_o(°C)		/10^5	Fr^*	Ma^*	T(°C)	z_x	v_R	Ma_o	ΔP_R	
9/17A a												
b	4.68	25.9	33.1	3.46	5.0	.60	24.4	1.23	2.14	.64	1.62	---
c	4.65	26.2	30.4	3.45	5.0	.60	23.8	1.90	2.80	.65	2.12	---
d	4.79	26.3	27.1	3.56	5.3	.61	22.3	3.11	4.10	.71	2.19	---
9/20A a												
b	4.64	26.4	34.4	3.45	5.0	.59	24.8	1.33	2.22	.63	1.68	---
c	4.67	26.6	31.4	3.48	5.1	.59	24.1	1.95	2.83	.65	2.20	---
d	4.81	26.6	28.5	3.58	5.4	.61	22.6	3.16	4.12	.71	2.29	---
9/21A a												
b												
c	4.85	27.1	29.1	3.66	5.5	.61	23.3	3.01	3.90	.71	2.49	---
d	5.02	27.4	23.8	3.77	5.9	.62	20.7	5.25	6.52	.80	7.25	---

Table B5 - Data Series II (cont.)

Run	$\dot{m}$(kg/s)	T_o(^oC)	$P_o-P_s(T_o)$ (kPa)	$Re^*/10^5$	Fr^*	Ma^*	T(^oC)	$\bar{z}_x$	v_R	Ma_o	ΔP_R	
9/28B a												
b	4.81	26.5	34.9	3.57	5.3	.61	23.9	2.01	2.90	.67	1.89	---
c	4.87	26.7	33.3	3.63	5.5	.62	23.2	2.72	3.63	.70	2.13	---
d	4.92	26.8	30.3	3.67	5.6	.62	22.4	3.45	4.42	.73	2.48	---

Table B6 - Data Series III

Run	$\dot{m}$(kg/s)	T_c(^oC)	$P_o-P_s(T_o)$ (kPa)	$Re^*/10^5$	Fr^*	Ma^*	T(^oC)	%x	v_R	Ma_o	ΔP_R	α(%)
9/29A a												
b	5.85	34.4	45.4	4.75	8.2	.62	29.5	4.00	4.14	.73	3.98	---
c	6.00	34.6	41.9	4.88	8.7	.63	27.2	5.97	6.06	.82	7.99	---
d	6.02	34.7	39.4	4.90	8.7	.63	26.0	6.96	7.15	.86	10.27	---
10/03A a												
b	5.55	34.4	35.2	4.50	7.4	.59	28.6	4.69	4.80	.72	4.42	---
c	5.72	34.6	31.7	4.66	7.9	.60	26.2	6.72	6.89	.81	9.00	---
d	5.74	34.8	28.2	4.68	7.9	.60	25.1	7.73	8.03	.84	12.14	---
10/03B a												
b	5.10	34.6	16.0	4.15	6.2	.54	27.1	6.04	6.13	.70	5.55	---
c	5.28	34.9	11.0	4.31	6.7	.55	24.6	8.15	8.52	.79	11.23	---
d	5.31	35.0	8.2	4.34	6.8	.55	23.3	9.23	9.90	.83	13.88	---

Table B6 - Data Series III (cont.)

Run	$\dot{m}$(kg/s)	T_o(^oC)	$P_o-P_s(T_o)$ (kPa)	$Re^*/10^5$	Fr^*	Ma^*	T(^oC)	$\bar{x}$	v_R	Ma_o	ΔP_R	α(%)
10/03C a												
b	4.87	35.1	16.2	3.99	5.7	.51	29.2	4.75	4.76	.62	3.19	---
c	5.22	35.3	9.85	4.29	6.6	.54	26.0	7.59	7.68	.75	9.15	---
d	5.33	35.8	6.22	4.39	6.9	.54	24.1	9.20	9.63	.82	12.90	---
10/04A a												---
b	4.74	34.2	28.6	3.84	5.4	.50	30.8	2.74	3.06	.56	3.06	---
c	4.88	34.4	26.4	3.96	5.7	.51	30.1	3.49	3.69	.60	2.38	---
d	5.14	34.5	22.5	4.18	6.3	.54	28.1	5.19	5.28	.68	4.41	---
10/04B	5.54	34.9	18.1	4.52	7.4	.58	23.8	8.74	9.29	.85	12.8	73.8
10/04C	5.21	35.7	11.6	4.29	6.6	.53	26.1	7.68	7.76	.75	8.25	73.9
10/04D	4.50	35.7	13.4	3.70	4.9	.46	30.5	4.25	4.24	.55	2.27	55.6

ABSTRACT

Despite the abundance of work in the field of two-phase flow, it seems as though a consensus has not been reached on some of the fundamental points. Although exceptions exist, adequate physical interpretation of the flow seems to be hindered either by complexity of analysis or, in the opposite extreme, the trend toward limited-range analysis and correlations. The dissertation presents the derivation of basic conservation equations for the phases. The combined equations are used to examine the phenomenon of "slip" and its practical limitations, the Fanno line for single-substance flow and the effect of slip on choking. Equations for critical mass flux in the presence of slip are derived. The Mach, Reynolds and Froude numbers based on conditions at flashing are introduced as the characteristic parameters, and the importance of compressibility in single-sub· ance two-phase flow is discussed. Experimental measurements of pressure change and void fraction for flow in the highly compressible range ($.5 < Ma < 1$) are presented. The working fluid is Refrigerant R-114, at room temperature, in a test section of diameter 5cm and length 8m. The effect of the Froude and Mach numbers is examined. The experimental facility is operated intermittently with running times of approximately two minutes and is instrumented for rapid measurements using a computer data acquisition and control system. A description of the facility and procedure is provided.